Sun Earth Connection Coronal and Heliospheric Investigation (SECCHI)

R.A. Howard, J.D. Moses, A. Vourlidas, J.S. Newmark, D.S. Socker, S.P. Plunkett, C.M. Korendyke, J. C. Cook, A. Hurley
E.O. Hulburt Center for Space Research
Naval Research Laboratory
Washington, DC 20375
USA

J. M. Davila, W. T. Thompson, O.C. St Cyr, E. Mentzell, K. Mehalick
NASA Goddard Space Flight Center
Greenbelt, MD 20742
USA

J.R. Lemen, J.P. Wuelser, D.W. Duncan, T.D. Tarbell
Lockheed Martin Space and Astrophysics Lab
Palo Alto CA 94304
USA

R. A. Harrison, N. R. Waltham, J. Lang, C.J. Davis
Space Science and Technology Dept.
Rutherford Appleton Laboratory
Chilton, Didcot, Oxfordshire OX11 OQX
UK

C.J. Eyles,
Astrophysics and Space Research Group
University of Birmingham
Edgbaston, Birmingham B15 2TT
UK

J.P. Halain, J.M Defise, E. Mazy, P. Rochus,
Centre Spatiale de Liège,
Université de Liège
Avenue du Pré-Aily
B-4031 ANGLEUR Belgium

R, Mercier, M. F. Ravet, F. Delmotte
Laboratoire Charles-Fabry de l'Institut d'Optique
91403 Orsay, France

F. Auchere, J.P. Delaboudiniere
Institut d'Astrophysique Spatiale
Centre universitaire d'Orsay
Bât 120 – 121
91405 ORSAY CEDEX, France

V. Bothmer,
University of Gottingen,
37077 Göttingen, Germany

W. Deutsch
Max-Planck-Institut for Solar System Research
Katlenburg-Lindau, Germany

D. Wang, N. Rich
Interferometrics, Inc
13454 Sunrise Valley Drive
Herndon, VA 20171
USA

S. Cooper, V. Stephens, G. Maahs
HYTEC Inc.
110 Eastgate Drive
Los Alamos, NM 87544
USA

R. Baugh, D. McMullin
Praxis, Inc
2550 Huntington Ave. Suite 300
Alexandria, VA, 22303

ABSTRACT

The Sun Earth Connection Coronal and Heliospheric Investigation (SECCHI) is a five telescope package, which has been developed for the Solar Terrestrial Relation Observatory (STEREO) mission by the Naval Research Laboratory (USA), the Lockheed Solar and Astrophysics Laboratory (USA), the Goddard Space Flight Center (USA), the University of Birmingham (UK), the Rutherford Appleton Laboratory (UK), the Max Planck Institüt für Solarsystemforschung (Germany), the Centre Spatiale de Leige (Belgium), the Institut d'Optique (France) and the Institut d'Astrophysique Spatiale (France). SECCHI comprises five telescopes, which together image the solar corona from the solar disk to 1 AU. These telescopes are: an extreme ultraviolet imager (EUVI: 1-1.7 $R_{\odot}$), two traditional Lyot coronagraphs (COR1: 1.4-4 $R_{\odot}$ and COR2: 2.5-15 $R_{\odot}$) and two new designs of heliospheric imagers (HI1: 15-80 $R_{\odot}$ and HI2: 80-215 $R_{\odot}$). All the instruments use 2048 x 2048 pixel CCD arrays in a backside mode. The EUVI backside surface has been specially processed for EUV sensitivity, while the others have an anti-reflection coating applied. A multi-tasking operating system, running on a PowerPC CPU, receives commands from the spacecraft, controls the instrument operations, acquires the images and compresses them for downlink through the main science channel (at compression factors up to 20x) and also through a low bandwidth channel to be used for space weather forecasting (at compression factors up to 200x). An image compression factor of about 10x will enable images to be collected at the rate of about one every 2-3 minutes. Identical instruments, except for different sizes of occulters, are included on the STEREO-A and STEREO-B spacecraft.

1 INTRODUCTION

The Sun-Earth-Connection Coronal and Heliospheric Investigation (SECCHI; see Howard et al., 2000) for the NASA Solar Terrestrial Relations Observatory (STEREO) mission is a suite of optical telescopes that will, for the first time, observe the entire inner heliosphere from the solar surface out to the vicinity of Earth. By combining this very large field of view with the radio and *in-situ* measurements from STEREO as well as from other space- and earth-based assets, we expect to answer some important questions of the physics of Coronal Mass Ejections (CMEs). The instrument acronym is also a reference to Angelo Secchi (1818-1878) a pioneering Italian astrophysicist who was one of the first to apply the new technology of photography to recording eclipses. In a similar way we anticipate that SECCHI will provide pioneering observations of CMEs as well as other structures, such as loops, plumes, streamers, comets, etc., using stereo deconvolution techniques.

The primary objective of the STEREO mission is to understand the CME phenomenon, a phenomenon that was discovered in 1971 and has been observed by coronagraphic instruments on five missions, most recently the NASA/ESA Solar and Heliospheric Mission (SOHO) (see Howard, 2006 and references therein). But, this is the first mission whose primary objective is to elucidate the CME itself. The primary objectives of SECCHI are:

- What is the timing of physical properties involved in CME initiation? What are the structures involved in the CME initiation?
- What is the 3-dimensional structure and kinematic properties of CMEs?
- What is the 3-dimensional structure of active regions, coronal loops, helmet streamers, etc?
- What are the critical forces controlling the propagation of CMEs in the corona and interplanetary medium?

The SECCHI instrument suite consists of five telescopes covering a broad range of fields of view, starting at the solar surface and extending all the way to the interplanetary space between the sun and Earth. The five telescopes are of 3 types. The first is an extreme ultraviolet (EUV) imager, EUVI that will image the solar chromosphere and low corona in four emission lines out to 1.7 $R_{\odot}$. The COR1 and COR2 telescopes are the second type and are visible light Lyot coronagraphs with nested fields of view. These two telescopes will image the inner and outer corona from 1.4 to 15$R_{\odot}$ and were split into two telescopes because of the large radial gradient of coronal brightness in this height range. The third type of telescope extends the coronal imaging from 15 $R_{\odot}$ out to the radius of Earth at 215 $R_{\odot}$. To satisfy the stray light requirement over this field, the task was divided into two wide field heliospheric imagers (HI1 and HI2). Figure 1-1 gives a summary of the science objectives and how each telescope in the SECCHI suite will contribute. EUVI and the CORs are instruments that have flown on previous missions, but the HI is a new concept.

STEREO provides us with several important new opportunities for CME research, including the following:

- The first opportunity to obtain stereographic views of CMEs;
- The first opportunity to observe a CME in interplanetary space at the same time that *in-situ* measurements are made;
- The first opportunity to make simultaneous optical and radio observations of CMEs and shocks;
- The first opportunity to observe geo-effective CMEs along the Sun-Earth line in interplanetary space;
- The first opportunity to detect CMEs in a field of view that includes the Earth.

In this paper we present an overview of the SECCHI instrument – the five main telescopes, the guide telescope (GT), the optical bench for the sun-pointed instruments (SCIP), the mechanisms, the SECCHI electronics, the CCD detector, housing and control electronics, the flight software and the concept of operations.

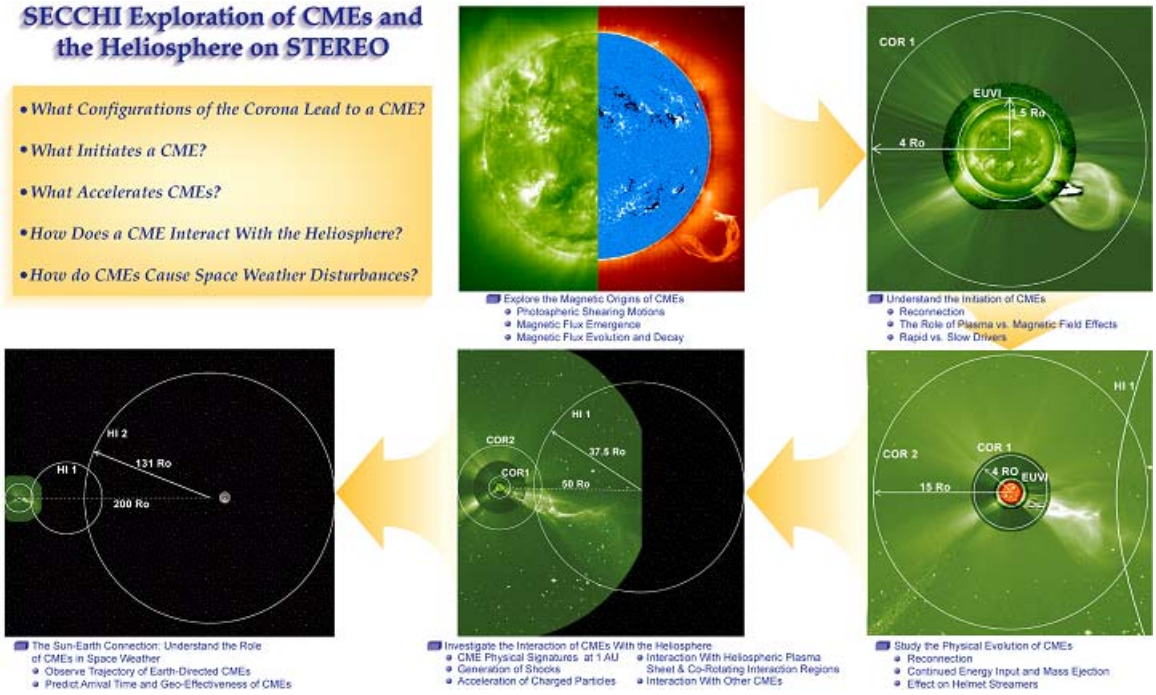

Figure 1-1. Summary of SECCHI Science Objectives

2 Extreme UltraViolet Imager (EUVI)

2.1 EUVI Telescope Overview

The EUVI telescope was developed at (LMSAL). The EUVI mirrors were figured and coated at (IOTA) and calibrated at (IAS), the focal plane assembly was developed at NRL and the University of Birmingham, the camera electronics were developed at RAL, and the aperture door was supplied by (MPS). The EUVI observes the chromosphere and low corona in four different EUV emission lines between 17.1 and 30.4 nm. It is a small, normal-incidence telescope with thin metal filters, multilayer coated mirrors, and a back-thinned CCD detector. Figure 2-1 shows one of the EUVIs during integration at LMSAL. Figure 2-2 is a cross section through the telescope.

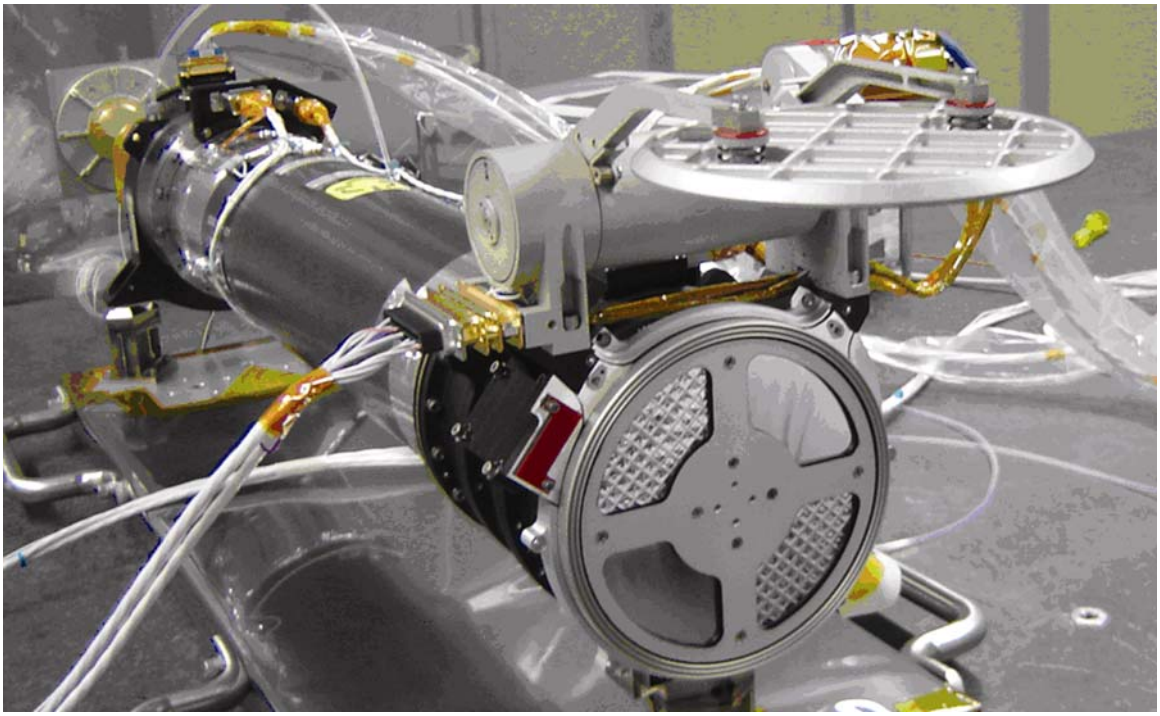

Figure 2-1 The EUVI telescope prior to integration into the SECCHI suite. The door is open and reveals the thin Al entrance filters. The bottom left and top right filters are mesh based filters, the others are polyimide backed supported on a coarse grid

EUV radiation enters the telescope through a thin metal film filter of 150 nm of aluminum. This filter suppresses most of the UV, visible, and IR radiation and keeps the solar heat out of the telescope. During launch, the filter is protected by the front door. The radiation then passes through the quadrant selector to one of the four quadrants of the optics. Each quadrant of the primary and secondary mirror is coated with a narrow-band, multilayer reflective coating, optimized for one of four EUV lines. After bouncing off the primary and secondary mirror, the radiation continues through a filter wheel that has redundant thin-film aluminum filters to remove the remainder of the visible and IR radiation. A rotating blade shutter controls the exposure time. The image is formed on a CCD detector. The main parameters for the EUVI telescope are summarized in Table 2-1.

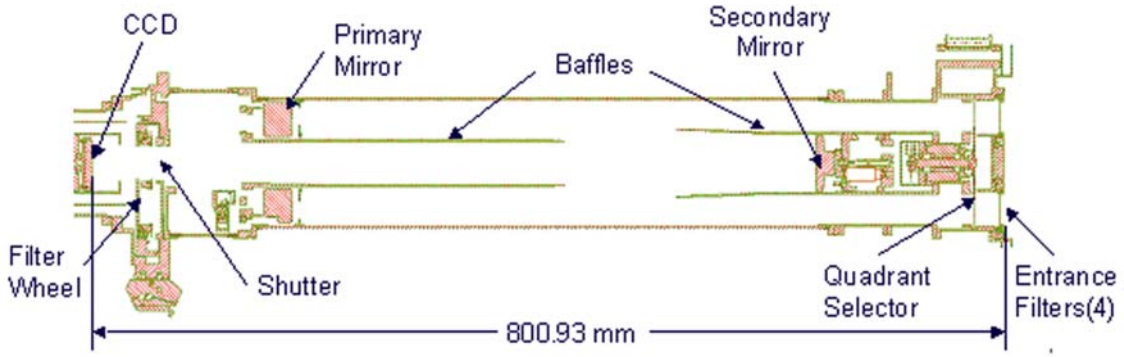

Figure 2-2. EUVI telescope cross section.

Table 2-1. EUVI Telescope Properties

Instrument Type	Normal incidence EUV telescope (Ritchey-Chrétien)
Wavelengths	He II 30.4 nm, Fe IX 17.1 nm, Fe XII 19. 5nm,Fe XV 28.4 nm
IR/visible/UV rejection	$> 10^{13}$ using thin metal film filters
Aperture	98 mm at primary mirror
Effective Focal Length	1750 mm
Field of View	Circular full sun field of view to ±1.7 solar radii
Spatial Scale	1.6” pixels
Detector	Backside illuminated CCD (e2v CCD42-40), 2048 x 2048 pixels
Mechanisms	Aperture door, Quadrant selector, Filter wheel,Focal plane shutter
Image Stabilization	Active secondary mirror (tip/tilt) Range: ±7”, jitter attenuation: factor 3 at 10 Hz

2.2 Optics

2.2.1 Optical Design

The EUVI telescope is a Ritchey-Chrétien system with a secondary mirror magnification of 2.42. This system provides pixel limited resolution across the entire field of view in all four quadrants. The low secondary mirror magnification reduces the telescope’s sensitivity to shifts in the mirror separation and eliminates the need for a focus mechanism. The telescope is fully baffled to prevent charged particles entering the front aperture from reaching the CCD. The telescope pupil is located just in front of the primary mirror and is defined by an aperture mask. The baffles and aperture mask have been designed for an unvignetted field of view to ±1.7 solar radii. Figure 2-3 shows ray trace results for a single quadrant, both on-axis and at the edge of the field, and up to 0.15 mm inside and outside of nominal focus. The system has a minor amount of field curvature; the nominal focus location is chosen to minimize the aberrations across the field.

2.2.2 Mirrors

The EUVI mirrors were figured, polished, and multilayer coated at the Institut d’Optique in Orsay, who also made the mirrors for SOHO/EIT. The Zerodur mirror substrates were first polished to a sphere and superpolished to the required surface roughness. They were then aspherized using an ion beam etching technique that preserves the superpolished properties of the surface. Finally, each quadrant of each mirror was coated with a narrow passband reflective multilayer, optimized for the specific EUV emission to be observed in that quadrant. All coatings consist of MoSi layer pairs. The coating for the 28.4 nm quadrant has a variable layer spacing for optimum suppression of the nearby 30.4 nm He II emission line. The other

coatings use constant layer spacings. Table 2-2 summarizes the properties of the coatings (Ravet et al, 2003).

Figure 2-3. Ray trace results for a single quadrant and two field angles (0 and 27 arcmin) at nominal focus, and up to 150 μm inside (–150) and outside (150) of nominal focus. The boxes indicate the size of one CCD pixel.

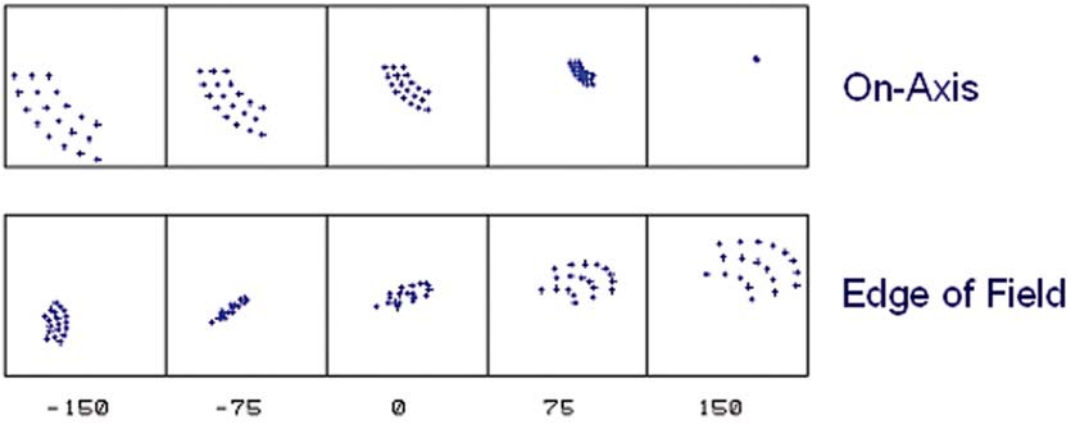

Table 2-2. Properties of the multilayer coatings.

Quadrant/Channel	**17.1**	**19.5**	**28.4**	**30.4**
Center wavelength (two mirror system)	17.3 nm	19.6 nm	28.5 nm	30.7 nm
Bandwidth (measured FWHM for single reflection)	1.4 nm	1.6 nm	1.9 nm	3.0 nm
Peak reflectivity (measured, for single reflection)	39 %	35 %	15 %	23 %
Coating materials	MoSi	MoSi	MoSi, var. spacing	MoSi

2.2.3 Filters

The EUVI uses thin metal film filters at both the entrance aperture and near the focal plane to suppress undesired UV, visible, and IR radiation. Two types of filters are at the entrance of the telescope (Figure 2-1): an aluminum-on-polyimide foil on a coarse nickel grid for the short wavelength quadrants (17.1 and 19.5 nm), and a single layer aluminum foil on a fine nickel mesh for the long wavelength quadrants (28.4 and 30.4 nm). Both types of filters use a 150 nm thick layer of aluminum to reject visible light. The grid-supported aluminum filter is backed with a 70 nm thick layer of polyimide for strength. The polyimide layer allows the filter to be supported by a coarse grid with 5 mm line spacing that causes only minimal diffraction at EUV wavelengths. The polyimide transmits only about 50% of the EUV radiation at the observing wavelengths, but this is not a major concern for the strong lines at 17.1 and 19.5 nm. The mesh supported filter avoids the absorbing polyimide layer, whose transmission is too low at longer wavelengths, especially for the somewhat weaker line at 28.4 nm. However, the fine mesh, with 0.36 mm line spacing, causes a noticeable amount of diffraction. Both types of filters have been flown on highly successful experiments: EIT used a plastic reinforced aluminum foil on a nearly identical coarse grid for all wavelengths and TRACE (Strong et al, 1994) used fine mesh supported filters nearly identical to the ones on the EUVI. Near the focal plane 150 nm thick aluminum filters on a fine mesh are housed in a filter wheel. The filter wheel offers redundant filters in case pinholes should develop on orbit. A third filter wheel position contains two filters in series to mitigate against any catastrophic damage to the entrance filters. The fourth filter slot is left open, primarily for ground testing. All filters were manufactured by LUXEL Corporation.

2.2.4 Aliveness Source

The EUVI telescope contains blue and violet light emitting diodes (LEDs) for testing and calibration purposes. One set of LEDs is mounted in the spider and illuminates the detector through reflection off the two telescope mirrors. A second set is mounted near the CCD. Photons from the blue LED at 470 nm have a similar penetration depth in silicon as EUV photons, while photons from the violet LED at 400 nm provide a diagnostic that is sensitive to CCD surface effects. Photons from the violet LED at 400 nm have a shallower penetration depth and may potentially provide a diagnostic for changes in the sensitivity of the surface layer of the CCD.

2.3 Mechanical Design

2.3.1 Metering Structure

The EUVI uses a Graphite/Cyanate Ester metering tube as the main telescope structure. The tube stiffness maintains proper alignment of the optical system through launch. The low coefficient of thermal expansion (CTE) in the axial direction minimizes changes in the mirror separation and keeps the telescope in focus throughout the operational temperature range. This eliminates the need for a focus mechanism. The metering tube is lined with an aluminum foil on the inside that acts as a vapor and contamination barrier.

Attached to the front of the metering tube are the secondary mirror spider, the quadrant selector spider, and the entrance chamber with the entrance filters and the interfaces to the aperture door and the forward mount. The spider arms are hollow and incorporate separate vent paths for the secondary mirror tip-tilt mechanism and for the quadrant selector motor. Attached to the aft end of the metering tube are the primary mirror mount and the aft metering structure with the shutter and filter wheel mechanisms, as well as the interfaces to the focal plane assembly and the aft mounts. The aft structure again incorporates separate vent paths for its mechanisms to minimize potential sources of contaminants inside the optical cavity.

2.3.2 Mirror Mounts

The EUVI primary mirror and mount are shown in Figure 2-4. The mount consists of a hexagonal Titanium ring that interfaces to the mirror substrate via three bi-pod flexures. This arrangement is semi-kinematic: each bi-pod strongly constrains two degrees of freedom, but is relatively flexible in the other four, thus isolating the mirror from thermal stresses in the mount. Interferometric tests showed that temperature changes of up to 22 C cause no measurable deformation of the mirror figure. The bi-pods are made of Invar and attach to the Zerodur mirror through bonded Invar mounting pads. This mirror mount is very compact to fit the tight envelope constraints of the EUVI telescope.

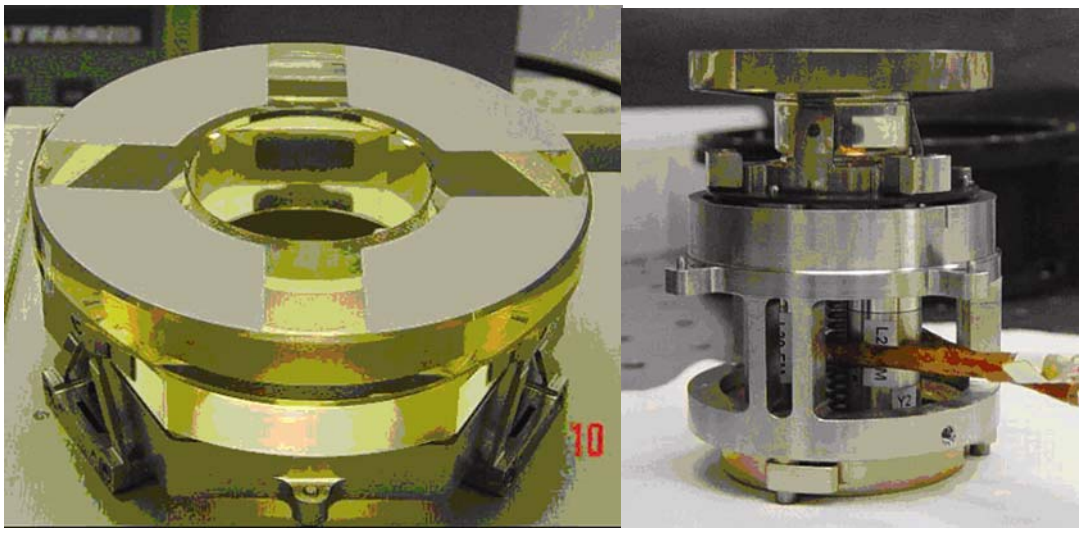

Figure 2-4. Left - EUVI primary mirror, coated and mounted. the mirror diameter is 105 mm. The regions between the quadrants are deliberately left uncoated. Right - EUVI secondary mirror and tip-tilt mechanism. The mirror diameter is 48 mm. One of the three PZTs (marked “L2...M”) is clearly visible inside the housing.

The secondary mirror mount with its tip-tilt mechanism is shown in Figure 2-4. The mount is a single piece of Invar with three machined fingers that are bonded to the cylindrical base of the Zerodur mirror substrate. The tip-tilt mechanism is very similar to the one on the TRACE telescope. It uses three piezoelectric (PZT) actuators that push against the Invar mount of the mirror. Software in the SECCHI flight electronics processes fine pointing signals from the SECCHI guide telescope and drives the PZT actuators open loop via a simple digital-to-analog converter and low voltage drivers. The tip-tilt range in the EUVI image space is ±7 arcseconds, sufficient to accommodate worst case spacecraft jitter.

2.3.3 Focal Plane Assembly[AV1]

The EUVI focal plane assembly (FPA) houses the e2v CCD42-40 detector and is passively cooled via an aluminum cold finger and a radiator surface at the anti-sun deck of the STEREO spacecraft. The FPA is equipped with a heater to keep the CCD warm during the time of high outgassing rates shortly after launch, and for occasional warmups for decontamination purposes and for annealing out radiation damage, if necessary. The FPA has its own vent path along the cold finger and through the radiator.

2.4 Instrument Response and Calibration

2.4.1 Calibration Results

The EUVI mirrors were calibrated as pairs at the synchrotron of the Institut d'Astrophysique Spatiale in Orsay. The mirrors were arranged in the same geometry as in the EUVI telescope, and illuminated with a nearly collimated beam from a monochromator attached to the synchrotron. Each telescope quadrant was measured individually. Wavelength scans were performed with and without the telescope in the beam; the measured ratio provides the absolute total reflectivity of the mirror pairs. Single reflection coating properties are reported in Table 2-3. All coatings perform well, both in terms of high reflectivity and proper wavelength of peak reflectivity. The coating for 28.4 nm is optimized for rejecting the strong He II line at 30.4 nm, which results in a somewhat lower peak reflectivity as expected.

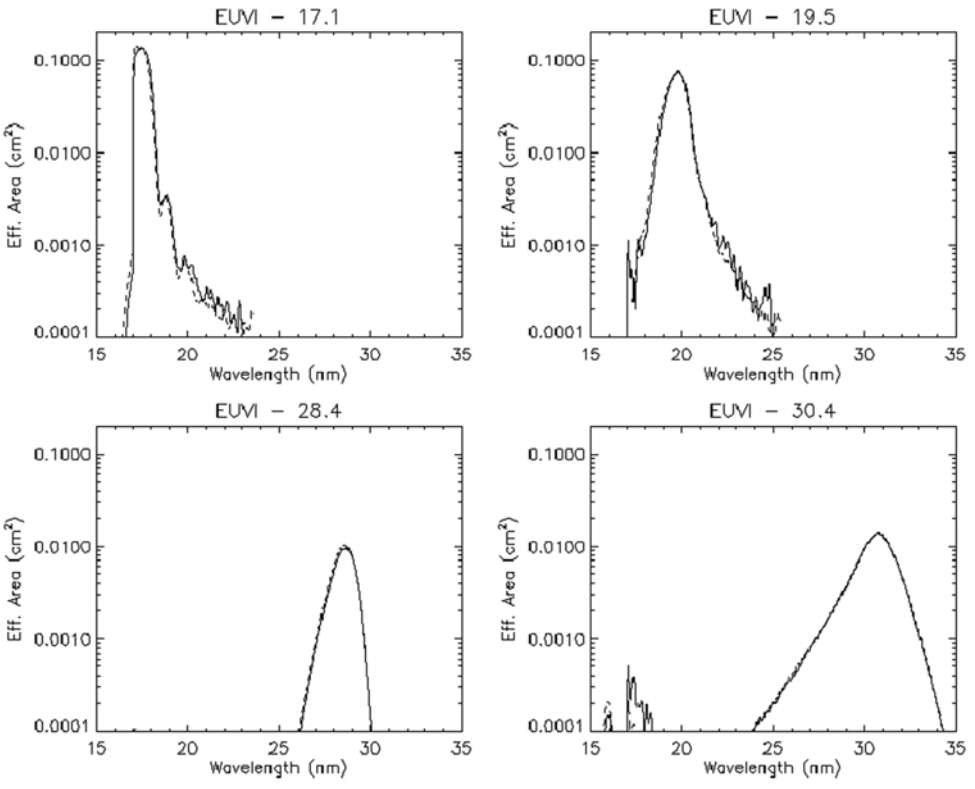

Figure 2-5. EUVI effective area. The solid lines are for the EUVI-A, the dashed lines for the EUVI-B.

CCDs were calibrated at the Brookhaven synchrotron and at the LMSAL XUV calibration facility. The entrance and focal plane filters were also calibrated at the LMSAL XUV calibration facility. The results of those measurements were used to fit CCD and filter response models. The calibration curves of the individual components were combined to obtain the EUVI effective area as a function of wavelength. The results are shown in Figure 2-5. The two telescopes (EUVI-A and EUVI-B) have very similar responses.

2.4.2 Predicted Response to Solar Phenomena

Using the calibration results we predict the response of the EUVI to typical solar plasmas. We take typical differential emission measure distributions (DEMs) reported in the literature, predict the resulting solar spectral line emission using the CHIANTI[8] software, and combine the result with our calibration data. Table 2-4 summarizes the pixel count rates for selected solar features in the different EUVI channels. Note that CHIANTI underestimates the He II flux by typically a factor of three so we have multiplied the prediction by a factor of 3. Figure 2-6 shows count rates predicted for isothermal plasmas as a function of plasma temperature.

Table 2-4. Photon count rates (phot/pixel/second) for some solar features predicted with the Chianti code. The numbers for the 30.4 nm channel have been tripled to adjust for the fact that Chianti typically underestimates the He II flux. The first number in each box is for the EUVI-A, the second for the EUVI-B

Photons/s/pixel	Quiet Sun	Active Region	M Class Flare
17.1 nm	92 / 98	954 / 976	25700 / 26700
19.5 nm	40 / 41	784 / 792	92200 / 101500
28.4 nm	4 / 4	118 / 130	5540 / 6110
30.4 nm	30 / 30	428 / 419	18100 / 17800

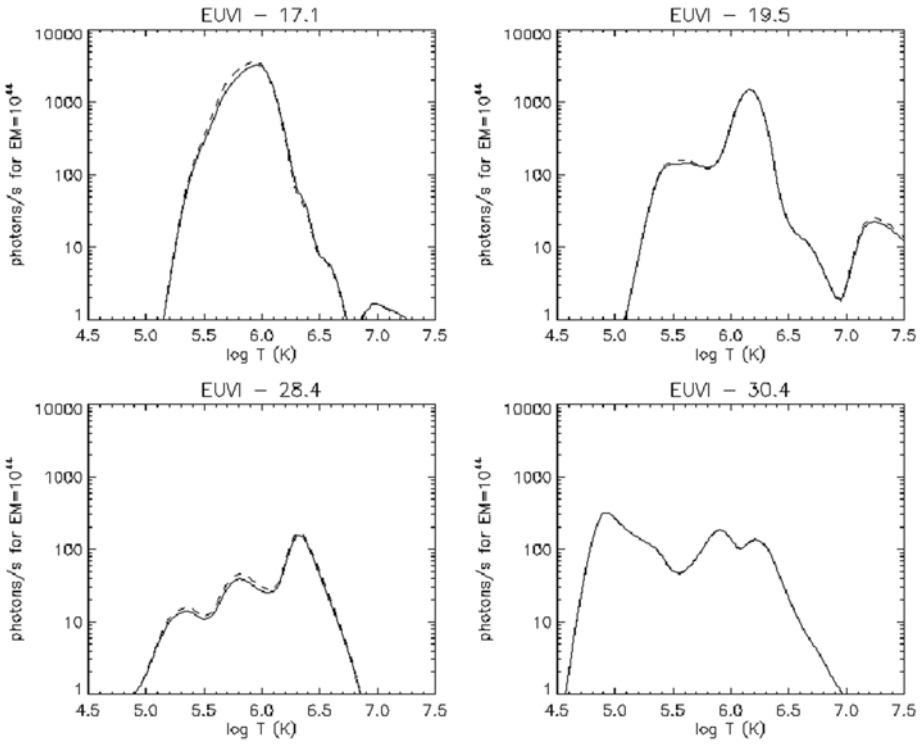

Figure 2-6. The response of the EUVI as a function of solar plasma temperature. The solid lines are for the EUVI-A, the dashed lines for the EUVI-B.

3 CORONAL IMAGING

3.1 COR1 Coronagraph

The SECCHI inner coronagraph, known as COR1, is a classic Lyot internally occulting refractive coronagraph (Lyot 1939), adapted for the first time to be used in space. The field of view is from 1.4 to 4 solar radii. A linear polarizer is used to suppress scattered light, and to extract the polarized brightness signal from the solar corona.

3.1.1 Optical Layout

Figure 3-1 shows the optical layout of the COR1 instrument. Sunlight enters through the front aperture, where the objective lens focuses the solar image onto the occulter. To keep scattering to a minimum, a singlet lens is used for the objective, made of radiation hardened BK7-G18 glass. The primary photospheric light suppression mechanisms in COR1 are the objective lens to occulter imaging system and the aperture stop to field lens to Lyot stop imaging system. Rather than relying on the out-of-band rejection of the filter, these primary suppression mechanisms are designed to work over the full sensitivity wavelength band of the instrument. The solar image from the objective will be chromatically aberrated, so the occulter must be sized to block all the solar photospheric light from the near UV to infrared (350-1100 nm). The cut-on at 350 nm is set by the transmission of the BK7-G18 glass in the objective lens, and the cut-off at 1100 nm is set by the band gap of the silicon detector. Subsequent lenses in the optical train balance the chromatic aberration from the objective. The narrow bandpass of the instrument also minimizes the effect of chromatic aberration in the final image

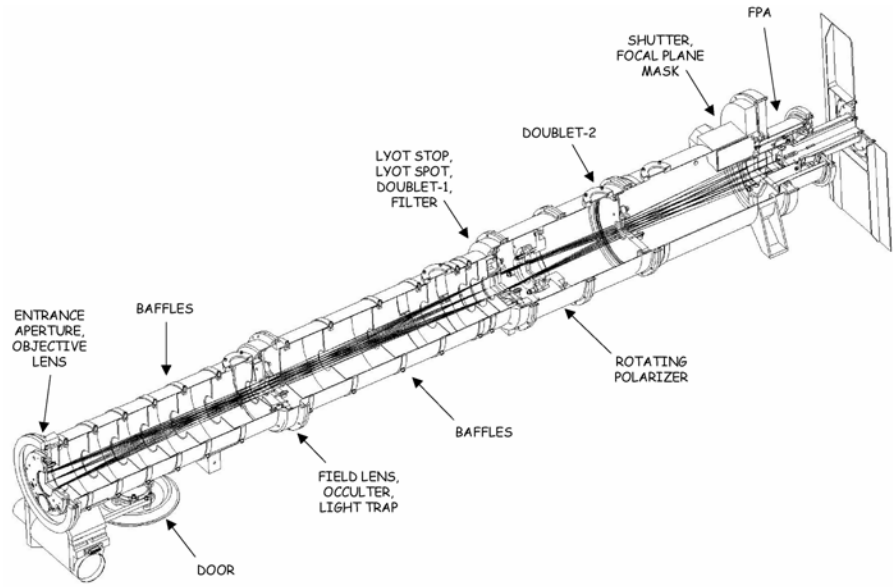

Figure 3-1. Layout of the COR1 instrument package

The occulter is mounted on a stem mounted at the center of the field lens (Figure 3-2}). The tip of the occulter is cone shaped, to direct the sunlight into a light trap, which surrounds the occulter. The radius was chosen to block all wavelengths (350-1100nm) out to a radius of 1.1 $R_{\odot}$ at orbital perigee. At the design wavelength of 656nm, the solar image is completely occulted out to 1.30 $R_{\odot}$, and partially vignetted out to 1.64 $R_{\odot}$. (When combined with the focal plane mask discussed below, these numbers become 1.4

and 1.9 $R_{\odot}$ respectively.) The wedge-shaped design of the light trap ensures that any ray entering it must reflect many times, so that the light will be absorbed before it can find its way out again.

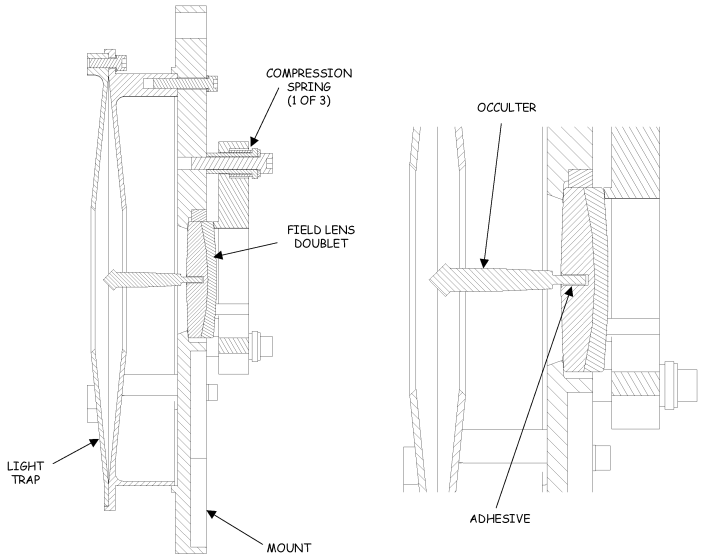

Fig 3-2. The conical occulter mounted at the center of the field lens, and surrounded by the light trap. Hashed regions show the presence of material at the central plane in this cutaway view.

Diffracted light from the edge of the front aperture is focused onto a Lyot stop and removed. This eliminates the largest source of stray light in the system. Additional stray light rejection is accomplished by placing baffles at various points between the front aperture and Lyot stop. A Lyot spot is also glued to the front surface of the doublet lens immediately behind the Lyot stop, to remove ghosting from the objective lens.

Two doublet lenses are used to focus the coronal image onto the CCD detector. The first, a positive power achromat, is placed immediately behind the Lyot stop, while the second, a negative power achromat, is placed further down the optical path. Together, these act as a telephoto-lens system, focusing the coronal image onto the detector plane, while maintaining diffraction-limited resolution. A bandpass filter 22.5 nm wide, centered on the Hα line at 656 nm, is placed just behind the first doublet. Thus, the Lyot stop, spot, first doublet, and bandpass filter form a single optical assembly.

A linear polarizer on a hollow core motor rotational stage is located between the two doublets. The polarizing material is Corning's Polarcor, chosen for its uniformity. The placement of the polarizer was chosen to be as close to the first doublet as possible within the dimension constraints of the largest diameter piece of Polarcor that can be obtained (33 mm clear aperture). Normal operations call for three sequential images to be taken with polarizations of 0° and ±60°, to extract the polarized brightness.

A focal plane mask is located between the shutter and the focal plane detector, and is used to remove diffracted light from the edge of the occulter. This circular mask, mounted on a plane of BK7 glass, is sized to be slightly larger than the occulter image at that location. Without the mask, the image on the detector would be dominated by bright rings at the umbral and penumbral edges of the occulter shadow. The addition of the focal plane mask removes these bright rings. The focal plane assembly is discussed in Section 9.

3.1.2 Mechanical and Thermal Design

The COR1 mechanical structure is designed as a series of tube sections (Figure 3-1), which are bolted and pinned together for stability. The individual optics are aligned, mounted, and pinned within these tube sections. COR1 assembly starts from the front tube section, with the objective, occulter, light trap, and field lens, and then each subsequent section is added, together with its associated optical or mechanical components. Because the individual tube sections are pinned together, sections can be taken off and back on again without changing the optical alignment.

Three mechanisms are included in the COR1 instrument package. At the front of the instrument is a door, , to protect the instrument before and during launch, and during spacecraft maneuvers. On the front of this door is a diffuser so that the operation of the instrument can be tested when the door is closed, and to provide a flat-field calibration signal. The diffuser is sized to completely illuminate the objective over all angles within the field-of-view.

The other two mechanisms are the hollow core motor to rotate the linear polarizer, and a rotating blade shutter mounted just in front of the focal plane detector assembly, both supplied by Lockheed Martin. All the mechanisms, together with the focal plane CCD detector, will be operated from a centralized control system for all the SECCHI instruments.

Because the two STEREO spacecraft are in elliptical orbits about the Sun, the COR1 instruments will experience considerable variation in solar load, from 1264-1769 and 1068-1482 W/m^2 for the Ahead and Behind spacecraft respectively. When these loads are combined with the modeled changes in the material thermal properties from beginning to end of life, and with the most extreme differences in the thermal loads from the surrounding structure, the worst-case temperature variation in the COR1 instrument is from 2.5 to 30° C. There's also an axial gradient in temperature from the front to the back of the instrument, varying from 3° C in the cold case, to 7° C in the hot case. Strategically placed software controlled proportional heaters with programmable set points, are used to keep the instrument within the 0-40° C operational temperature range. There are also survival heaters on mechanical thermostat control to keep the instrument within the -20 to +55° C non-operational range.

Specialized composite coatings of oxides over silver are used to help manage the intense solar fluxes which COR1 will be experiencing. The oxide coatings are deposited onto many of the exposed surfaces around the aperture area, such as the objective lens holder assembly and door assemblies. This coating exhibits very low solar absorbtivities, is very stable, and has relatively high IR emissivity values depending on the thickness of the deposited oxide layers. Silver teflon is used for the front layer of the multilayer insulation. The majority of the solar load collected by the front objective is concentrated on the occulter tip (Figure 3-2). In the worst-case analysis, the tip can reach a temperature of 125° C. This tip is made of titanium, and is diamond turned to direct the sunlight into the light trap. It is coated with a Goddard composite silver coating for high reflectivity. The occulter shaft is coated with black nickel to radiate away the heat. A thin cross-section titanium shaft is used to thermally isolate the occulter from the field lens.

3.1.3 Calibration and Performance Results

Before building the COR1 flight units, an extensive test program was carried out on a series of breadboards and engineering test units, using the Vacuum Tunnel Facility at the National Center for Atmospheric Research in Boulder, Colorado (Thompson et al 2003). These tests were used to demonstrate the instrument concept, and to improve the design for flight. One result of this testing was the addition of a focal plane mask to remove diffracted light from the edge of the occulter.

Characterization of the COR1 flight units was carried out in a similar vacuum tank facility at the Naval Research Laboratory in Washington, D.C. The instrument was installed in a large vacuum chamber within a class 10,000 cleanroom. A long vacuum tunnel extended out from one end of the vacuum chamber to a window, where an entrance aperture was mounted to simulate the size of the Sun at perigee. The total distance between the source aperture and the COR1 front aperture was 11 meters. A partially collimated Xenon arc lamp was used to illuminate the source aperture, with the degree of collimation chosen to direct

the light onto the COR1 objective and heat shield. Different aperture sizes were used for the Ahead and Behind instruments, because of the different orbital perigees of the two spacecraft.

As well as stray light, this vacuum tunnel facility was also used to measure other performance characteristics, such as resolution, polarization, and photometric response. The photometric calibration of the instrument was measured by illuminating the aperture at the end of the tank with a diffuse unpolarized light source of known intensity. Placing a sheet polarizer in front of this source allowed us to test the polarization response. Focus was tested by projecting an Air Force 1951 resolution test target through a collimator onto the instrument. The instrumental flat field was tested using both the diffuser mounted in the door, and with an external double-opal source mounted in front of the instrument, with identical results.

The vignetting function and flat field response of the instrument is demonstrated in Figure 3-3. The field is unvignetted except for a small area around the edge of the occulter, and near the field stop in the corners of the image. (The dim spot in the center of the occulter shadow is caused by scattering within the instrument.) Only the Ahead data are shown-the Behind response is virtually identical.

Fig 3-3. Flat field response of the COR1 Ahead instrument.

Figure 3.4 shows the measured COR1 scattered light performance for the Ahead and Behind instruments. The average radial profile is well below 10^{-6} $B/B_{\odot}$ for both instruments. There are discrete ring-shaped areas of increased brightness, which can climb to as high as 1.4×10^{-6} $B/B_{\odot}$ for the Behind instrument. It has been determined that these are caused by features on the front surface of the field lens.

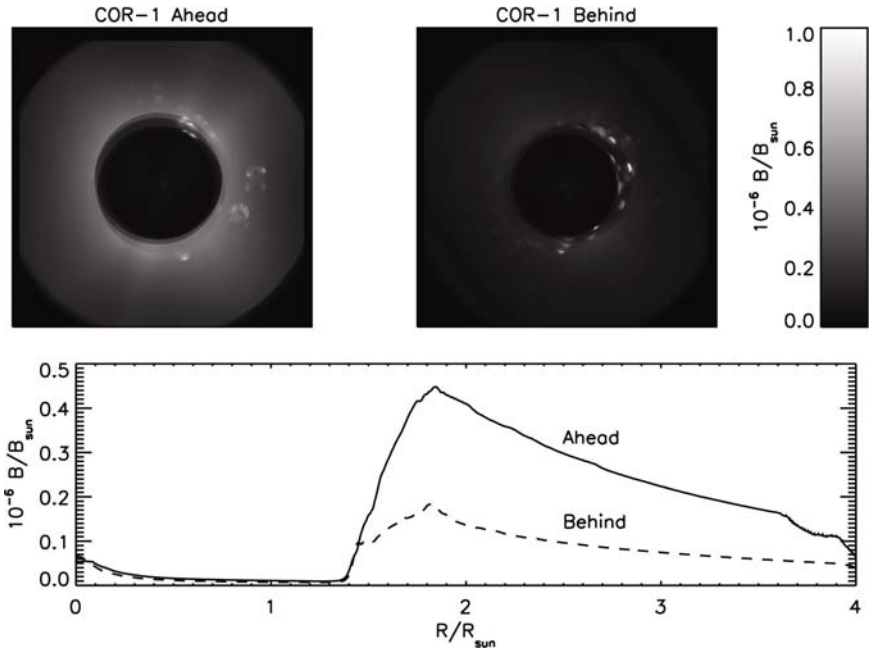

Fig 3-4 Measured scattered light images and average radial profiles for the COR1 Ahead (solid) and Behind (dashed) instruments.

Some contamination was found on the COR1 Behind objection after thermal vacuum testing of the STEREO spacecraft. The objective has been cleaned and re-installed, and may no longer have the performance shown in Figure 3-4.

Combining the data from Figures 3-3 and 3-4, together with a model of the K corona polarized brightness, allows one to estimate the signal-to-noise ratios that will be seen during flight. The results are shown in Figure 3-5 for an exposure time of 1 second. The coronal model used is based on Gibson (1973), is valid between 1.4 and 4 solar radii and has the functional form:

$$\log_{10}(pB) = -2.65682 - 3.55169\ (R/\ R_{\odot}) + 0.459870\ (R/R_{\odot})^2,$$

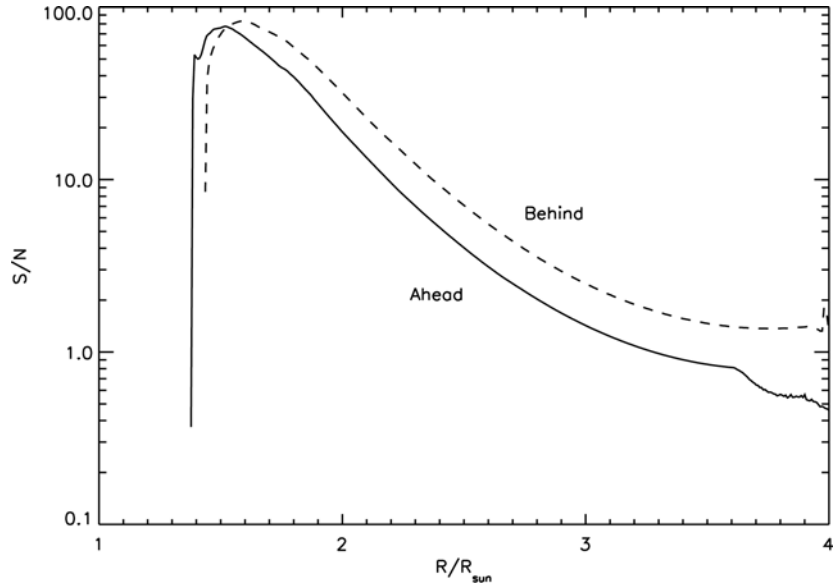

Fig 3-5 Estimated signal-to-noise ratios for a modeled K-corona for an exposure time of 1 sec, with 2x2 pixel binning.

The overall performance characteristics of the COR1 instruments are summarized in Table 3.1.

Table 3- 1 COR1 Performance Characteristic

Parameter	Units	Ahead	Behind
Pixel size, full resolution	arcsec	3.75	3.75
Pixel size, 2×2 binned	arcsec	7.5	7.5
RMS spot size (design)	arcsec	4.17	4.17
Planned exposure time	sec	1	1
Polarizer attenuation	-	10^{-4}	10^{-4}
Photometric response	$B_{\odot}$/DN	$7.1\ 10^{-11}$	$5.95\ 10^{-11}$
Time to complete pB sequence	sec	11	11
Image sequence cadence	min	8	8

3.1.4 Concept of Operations

Like all coronagraphs, COR1 is designed to measure the weak light from the solar corona in the presence of scattered light from the much brighter solar photosphere. The COR1 signal will be dominated by instrumentally scattered light, which must be removed to measure the underlying coronal signal. To build up enough signal to make this happen, the 3.75 arcsec square pixels will be summed together into 2x2 bins, to form larger pixels 7.5 arcsec on a side. The design goal for the root-mean-square spot size on the detector was chosen to be 15μm (4.17 arcsec), somewhat larger than the 13.5 μm size of a single CCD pixel, but well within the 27 μm size of a 2x2 binned pixel. The largest contribution to the optical error budget comes from thermal changes on orbit, which can be as large as 12 μm.

COR1 will measure both the total brightness B, and the polarized brightness pB, of the solar K corona. This is done by taking polarizer measurements at angles of -60°=I_a, 0°=I_b, and +60°= I_c, and combining them using the following equations (Billings 1966):

$$B = 2\ (I_a + I_b + I_c)$$
$$pB = (4/3)\ [(I_a + I_b + I_c)^2 - 3(I\_a\ I\_b + I\_a\ I\_c + I\_b\ I\_c)]½$$

The three images will be taken in sequence, as quickly as possible, so that changes due to evolution of the corona will be minimized. Each set of three images makes up a complete observation, and the cadence of observations is the time between one three-image set and the next.

3.2 COR2 Coronagraph

The SECCHI outer coronagraph, known as COR2, is an externally occulted Lyot coronagraph. COR2 derives its heritage from the highly successful LASCO C2 and C3 coronagraphs aboard SOHO (Brueckner et al 1996). It was designed and built by the Naval Research Laboratory. In comparison to LASCO, several design challenges were associated with COR2. The instrument was to have approximately the same field of view as LASCO C2 and C3 combined, a spatial resolution comparable to C2, a much shorter exposure time than either C2 or C3 while accommodating a greater bore sight offset from sun center and fitting into a smaller envelope.

3.2.1 Optical Design

Adequate K-corona signal detection in the faint outer C3 like portion of the field of view requires high exposure and minimal scattered light production at O1 & O2. High levels of diffracted light originating at the external occulter and localized in the final image near the inner 2.0-2.5 $R_{\odot}$ inner field of view cut off would both saturate the CCD before an adequately high exposure is achieved and increase scattered light production by O1 and O2. A related concern is the need to accommodate the expected COR1/COR2 bore sight offset and spacecraft jitter. We addressed these issues by paying particular attention to external occulter diffraction. Two diffraction models were developed and validated with laboratory tests. The models allow diffracted light level to be calculated accurately and minimized for a given inner field of view cutoff by adjustment of the diameters of the first two disks of a three-disk occulter system.

In addition to the diffraction modeling and testing, we also paid close attention to another source of instrumental background in the design phase: ghost images of the bright diffraction sourcing at the external occulter. Ghost images are formed by internal reflections of light from the bright edge of the final external occulter disk in the coronagraph, primarily in the O1 lens and secondarily by reflections from the CCD back toward the lens system. By careful control of lens surface radii in the optical design phase, we were able to confine all significant ghost images present at the focal plane to regions outside the CCD photosensitive area.

The CME velocity driven image smear over the required three polarization image sequence needed a high light gathering power design. In comparison to LASCO a shorter exposure time was achieved by using a CCD with a higher quantum efficiency (80% vs 36%), increasing the light gathering power by using a 34 mm A1 aperture rather than 20 mm (C2) or 9 mm (C3) apertures, and substituting Polarcor polarizing glass for Polaroid plastic sheet in the linear polarization analyzer which provides better matching of the solar spectral distribution peak to the CCD spectral responsivity.

The need for C2-like spatial resolution in combination with the 15 $R_{\odot}$ field of view (C2 = $7R_{\odot}$) was accomplished in part with a 2k x 2k CCD. The f-ratio was set to f/5.6 to avoid a substantial increase in instrument length that would be required to accommodate the larger A1 at the same f-ratios used for C3 (f/9.3) and C2 (f/20). Because the large A1 aperture, wide field angle and high spatial resolution placed a burden on the design of the lens system, particularly the O2 lens group, a tight tolerance precision potted lens system was used throughout the instrument.

3.2.2 Mechanical and Thermal Design

The COR2 mechanical layout is shown in Figure 3-6. The mechanical structure consists of a series of circular cross-section tubes. The tubes are mechanically aligned; match drilled, and pinned to allow for repeatability in assembly. There are a total of four primary tubes for mounting the optics and the FPA tube section. The tubes are fabricated from 6061-T6 aluminum. The COR2 instrument interfaces with the SCIP optical bench via a kinematic mount system comprising of three titanium flexures. The fundamental frequency of the structure with the kinematic mounts is 92 Hz. The COR2 instrument weighs approximately 11 kg and is 1.4 m long.

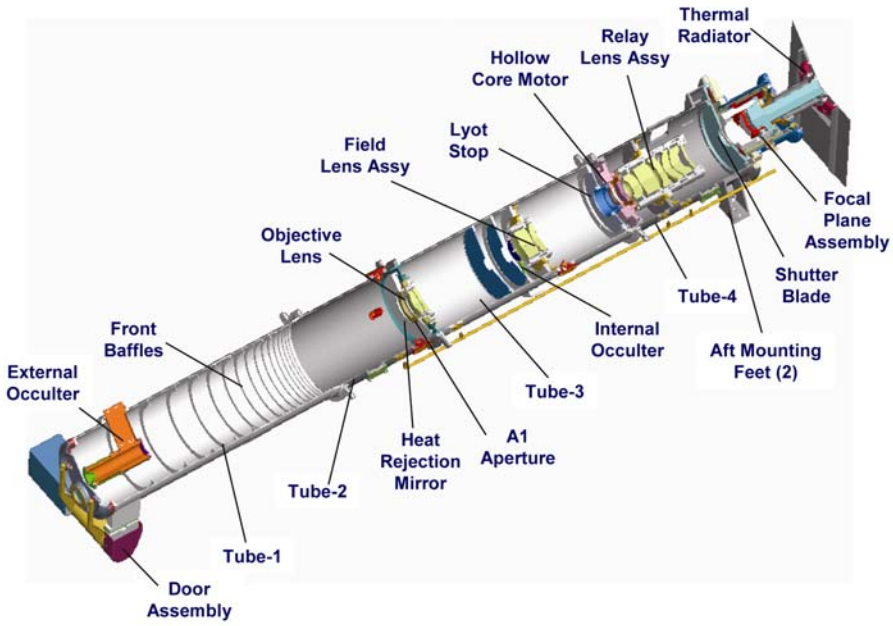

Fig. 3-6. COR2 Mechanical Layout

The first tube section, Tube 1, supports the door assembly, the A0 aperture, and the external occulter subassembly. Tube 1 is machined with internal baffles to reduce stray light entering A1. The tube incorporates a stiffening ring locally where it interfaces the front flexure for additional stiffness. The external occulter subassembly is cantilevered off the tube wall with a single pylon to reduce diffraction. The occulter system consists of three highly precision machined disks mounted on a spool. Tube 2 serves as additional metering length for the coronagraph.

At the interface of Tube 2 and 3, the objective lens assembly is integrated. The assembly consists of the heat rejection mirror, the A1 stop, and the objective lens set. Tube 3 supports two additional apertures, namely the Coronal and A0 Image, and the field lens set. The internal occulter and the Lyot Stop is also mounted to Tube 3.

Tube 4 supports the hollow core motor, the relay lens set, the shutter mechanism, and the FPA. The tube is machined with mounting feet to attach the two aft flexures. The FPA supports the CCD and the radiator. The radiator has a clear view to space and passively cools the CCD. The CCD is coupled to an Invar strongback for rigidity and mounted in a decontamination cup with a conductive path through the cold finger.

The COR2 thermal design is similar to COR1 in that it uses a slightly cold biased design. MLI blankets from the SCIP closeout insulate the instrument from its surroundings. The instrument temperature is maintained using a combination of thermostatically controlled survival heaters and PID controlled operational heaters. The structural tube surfaces are treated with an inorganic black anodize. This surface finish provides an optical black and increases thermal coupling within the instrument, reducing thermal gradients.

When the aperture door opens, some of the components comprising the front end of the instrument are exposed to the solar environment. Structural surfaces exposed to direct sunlight are coated with CCAg to prevent overheating. All other surfaces are black anodized to minimize scattered light. The heat rejection mirror, mounted in front of the objective lens, reflects the incident solar radiation back through the A0 aperture and into space.

The FPA outer housing and support structure is fabricated from titanium 6AL-4V for its thermal isolation characteristics. The radiator and cold finger are fabricated from 6063-T52 aluminum for optimal mass and conductivity.

3.2.3 Calibration and Performance Results

The COR2 calibration plan involved testing in both the component and telescope levels. The properties of the linear polarizers were measured in the lab and the two best polarizers were chosen for the flight instruments. The bandpass filters were manufactured and measured by Andover. The bandpass response was verified at NRL and again the best filters were used in the flight instruments. The most extensive component-level testing was performed on the various lens sets of the COR2 optical train. A breadboard version of the instrument was constructed to mount the 3 lens groups and to allow us to verify the optical prescription. With the aid of an Air-Force target, we were able to measure the MTF at various field angles and choose the lens group combinations with the best imaging performance.

The flight unit performance was measured at the NRL's Solar Coronagraph Test Chamber (SCOTCH) facility (Morrill et al 2006), the same facility used for the COR1 calibration (section 3.1.3) and under similar configuration. The instrument vignetting function and spectral response were measured in air. The stray light levels, image quality and absolute calibration were measured under vacuum. The tests were based on similar tests for the SOHO/LASCO coronagraphs and used the same or with very similar GSE.

The COR2 vignetting pattern for the Ahead telescope is shown in Figure 3.7. The image is vignetted throughout the field of view reaching a minimum of 20% at about 10 $R_{\odot}$ before increasing again towards the edge. The vignetting around the occulter pylon is only about 40-50% which does not impede imaging and therefore the pylon will be invisible in the images similarly to LASCO/C2.

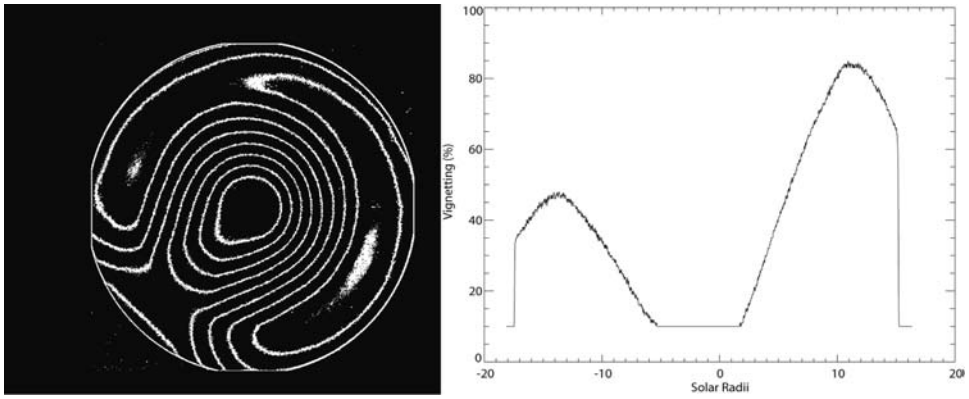

Fig. 3-7. Flat field response of the COR2 Behind instrument

The main improvement of the COR2 design over the LASCO C2 and C3 coronagraphs is the imaging of a combined C2 and C3 field of view with the C2 spatial resolution and the C3 stray light performance. The stray light tests (Figure 3.7) showed that the instrument performance exceeds the design requirements and will allow us very detailed imaging of the extended corona.

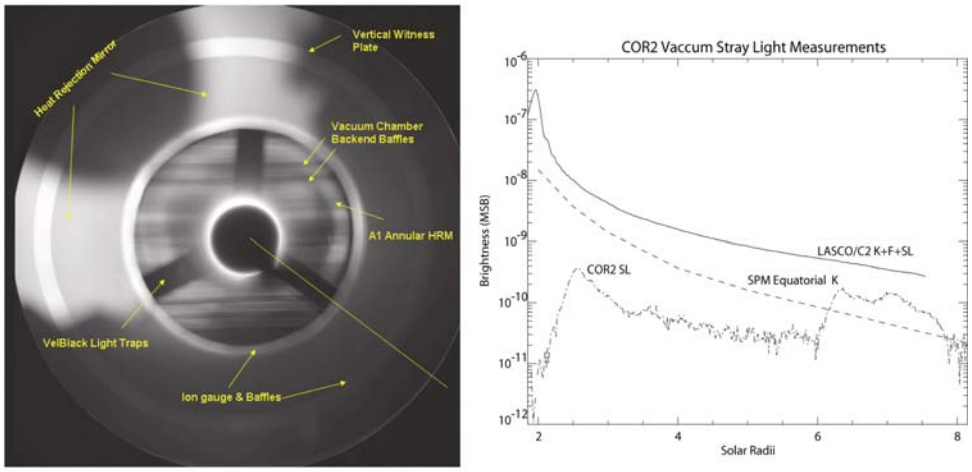

Fig 3-9. Stray light performance of the COR2 Behind instrument.

The overall performance characteristics of the COR2 instruments are shown in Table 3-2.

Table 3- 2 COR2 Performance Characteristics

Parameter	Units	Ahead	Behind
Pixel size, full resolution	arcsec	14.7	14.7
RMS spot size (design)	arcsec	15	15
Planned exposure time	sec	1	1
Polarizer attenuation	-	10^{-4}	10^{-4}
Photometric response	$B_{\odot}$/DN	$1.35\ 10^{-12}$	$1.25\ 10^{-12}$
Time to complete pB sequence	sec	11	11
Image sequence cadence	min	15	15

3.2.4 Operations

The COR2 instruments will acquire only polarized images of the corona since the polarizer is always in the beam. The standard sequence will be three images at -60°, 0°, and +60°, similar to COR1. All three images will be transmitted to the ground and then combined to produce total and polarized brightness images for further analysis. A low resolution, total brightness image created by the summation of the three polarized images will also be calculated onboard and transmitted thought the beacon channel. An alternative observation mode is to take two images at 0° and 90° in rapid succession without reading out the CCD in between exposures. This so-called "double" exposure corresponds to a total brightness image and is transmitted to the ground as a single image. This is useful way to save telemetry and increase image cadence for special observations. More details about the instrument operations are given in section 11.

4 The Heliospheric Imagers (HI)

4.1 Instrument Concept

HI consists of two small, wide-angle telescope systems mounted on the side of each STEREO spacecraft, which view space, sheltered from the glare of the Sun by a series of linear occulters. The HI instrument concept was derived from the laboratory measurements of Buffington et al. (1996) who determined the scattering rejection as functions of the number of occulters and the angle below the occulting edge. The result of their analysis showed that a simple telescope in a small package could achieve the required levels of rejection by proper occulting and by putting the telescope aperture sufficiently in the shadow of the occulter. The concept is not unlike observing the night sky after the Sun has gone below the horizon. Validation for this instrument concept comes the Zodiacal Light Photometer Pitz et al., 1976) [Pitz, E., C. Leinert, H. Link, and N. Salm, HELIOS zodiacal light experiment, in IAU Colloq. 31: Interplanetary Dust and Zodiacal Light, pp. 19-23, 1976.] on the Helios spacecraft, launched in 1974, and from the Solar Mass Ejection Imager (SMEI) instrument (Eyles et al., 2003), on the Coriolis spacecraft, launched in 2003. Both instruments have demonstrated that CMEs can be observed optically against the more intense background of zodiacal light and stars (Jackson & Tappin et al. 2000).

The basic design concept for HI can be seen in Figure 4-1. The instrument is a box shape, of major dimension about 700 mm. A door covers the optical and baffle systems during launch and the initial cruise phase activities. The one-time door is opened after all contamination generating spacecraft propulsion events have occurred prior to insertion into heliocentric orbit. The two telescope/camera systems, known as HI-1 and HI-2 are buried within a baffle system as shown in Figure 4-1. The direction to the Sun is shown; the Sun remains below the vanes of the forward baffle system. The detectors are CCD devices, which are passively cooled by radiating away the heat to deep space.

The performance specifications for HI are listed in Table 4-1. The HI-1 and HI-2 telescopes are directed to angles of about 13° and 53° from the principal axis of the instrument, which in turn is tilted upwards by 0.33 degrees to ensure that the Sun is sufficiently below the baffle horizon. Thus, the two fields of view are nominally set to about 14 and 54 degrees from the Sun, along the ecliptic line, with fields of view of 20 and 70 degrees, respectively. This provides on overlap of about 5 degrees.

In order to extract the CME signal from the much more intense background of Zodiacal light and stellar background, the SNR must be increased over a single exposure. This is accomplished by summing individual exposures on-board. This requires that the individual images be scrubbed for cosmic rays, prior to summing and also prior to being 2x2 pixel binned. This 2x2 binning results in angular sizes of 70 arcsec (HI-1) and 4 arcmin (HI-2) per pixel. The combination of summing 50 images and 2x2 binning results in an increase in the SNR of about 14x. For each telescope, Table 4-1 lists a nominal exposure time range and typical number of exposures per summed image. Since there is no shutter, a smearing will occur during the readout. Software to remove this effect was applied to images taken during thermal-vacuum testing with excellent results.

Table 4-1 – Performance Specifications of the HI Telescopes

	HI-1	HI-2
Direction of Centre of FOV	13.98 degrees	53.68 degrees
Angular Field of View	20 degrees	70 degrees
Angular Range	3.98-23.98 degrees	18.68-88.68 degrees
Image Array (2x2 binning)	1024x1024	1024x1024
Image Pixel Size	70 arcsec	4 arcmin
Spectral Bandpass	630-730 nm	400-1000 nm
Nominal Exposure time	12-20 s	60-90 s
Nominal Exposures Per Image	70	50
Nominal Image Cadence	60 min	120 min

Brightness Sensitivity (B_o = solar disk)	3×10^{-15} B_o	3×10^{-16} B_o
Straylight Rejection (outer edge)	3×10^{-13} B_o	10^{-14} B_o

The geometrical layout of the fields of view of the SECCHI instruments is shown in Figure 4-2. The HI-1 and HI-2 fields provide an opening angle from the solar equator at 45°, chosen to match the average size of a CME. The configuration provides a view of the Sun-Earth line from the STEREO coronagraph fields to the Earth and beyond. It should be remembered that this is done from two spacecraft at equal planetary angles (Earth-Sun-spacecraft), providing a stereographic view.

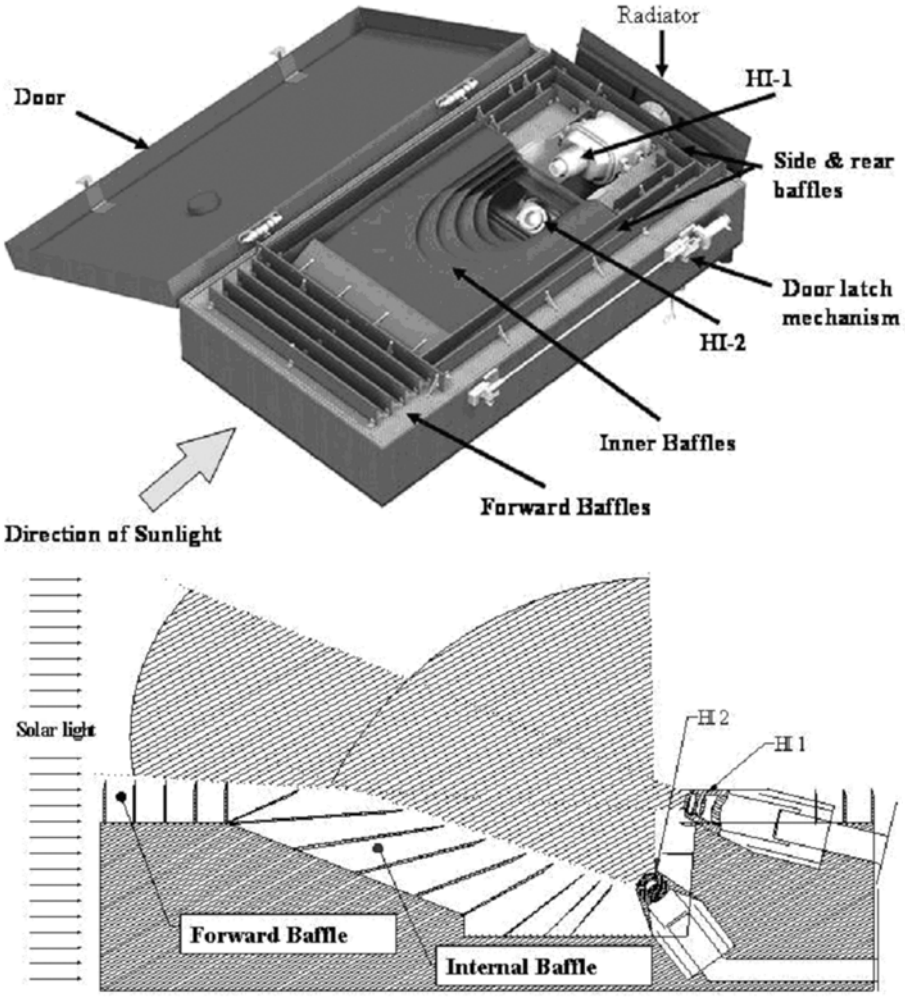

Figure 4-1. Top: The Heliospheric Imager design concept. Bottom: A schematic side view of the optical configuration, demonstrating the two fields of view of the instrument.

Figure 4-2 also indicates some of the major contributions to the intensities, which will be recorded by the HI instruments, in particular the F-corona (zodiacal light) and stellar intensities, as well as anticipated CME intensities. Note that the F-coronal intensity is about two orders of magnitude brighter than the CME signal.

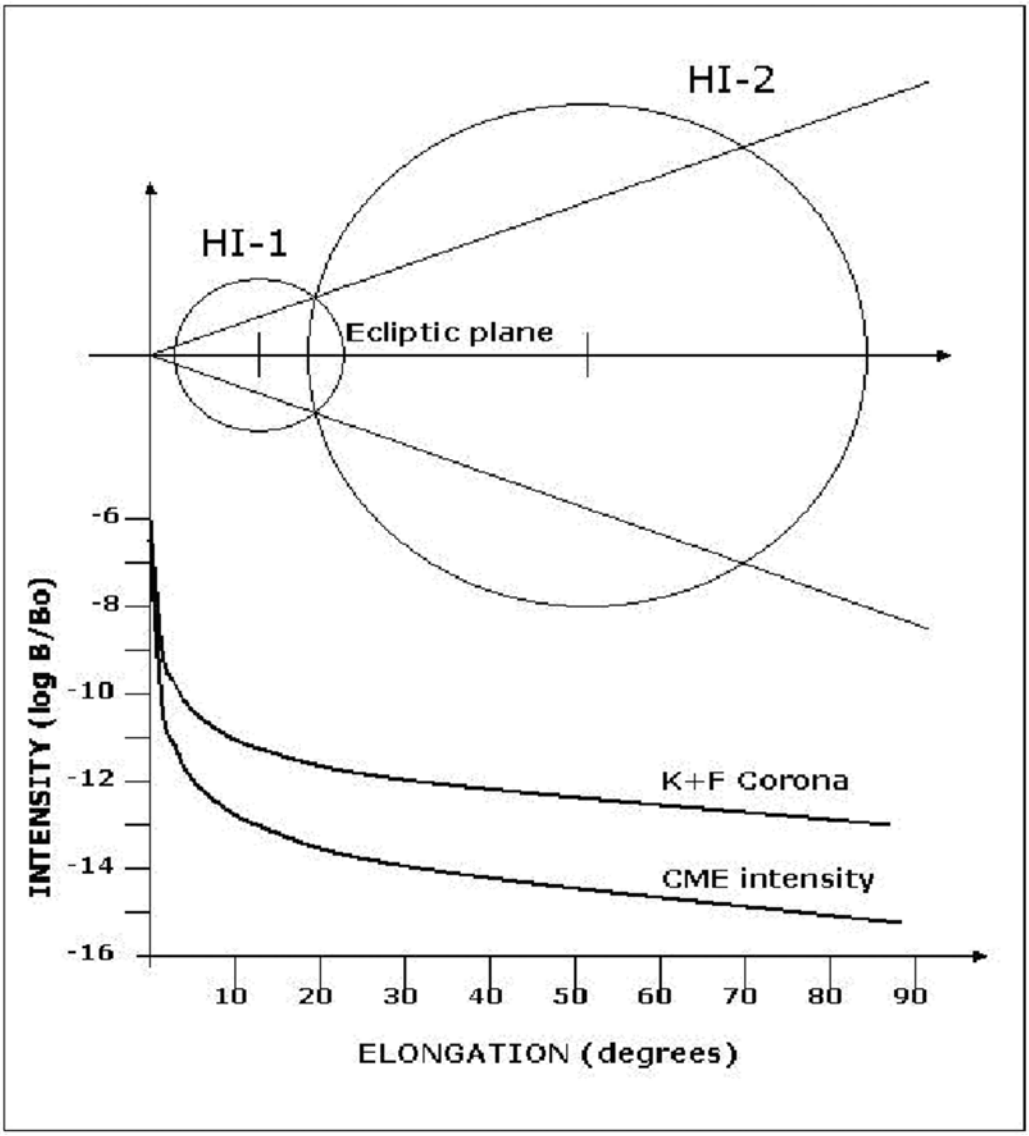

Figure 4-2 - The geometrical layout of the HI fields of view and the major intensity contributions (based on a figure from Socker et al. 2000).

The anticipated instrument stray light level must be at least an order of magnitude less than the F-coronal signal which can be seen, from Figure 4-2, to require levels of better than ~10^{-13} $B_{\odot}$ for HI-1 and ~10^{-14} $B_{\odot}$ for HI-2. In contrast, the brightness sensitivity requirement is based on the need to extract the CME signal from the other signal sources, which demands the detection of CME intensities down to 3 x 10^{-15} $B_{\odot}$ and 3 x 10^{-16} $B_{\odot}$.

The principal hardware development for HI was centred at Birmingham University, with camera design and development work and some thermal work provided by the Rutherford Appleton Laboratory. The Centre Spatial de Liege, Belgium, provided optical design, analysis and test effort. Numerous aspects of the assembly, integration and test work, and the overall SECCHI management overseeing the HI activities have been performed by the US Naval Research Laboratory. The HI concept was developed by Dennis Socker of the Naval Research Laboratory.

4.2 Baffle Design

The baffle design is the key to the HI concept. As shown in Figure 4-1, the baffle sub-systems consist of a forward baffle, a perimeter baffle and the internal baffle system. The forward baffle is designed to reject the solar disk intensity, reducing straylight to the required levels. The perimeter baffle is principally aimed at rejecting straylight from the spacecraft, and the internal baffle system is aimed at rejecting light from the Earth and stars. The forward baffle protects the HI-1 and HI-2 optical systems from solar light using a knife-edge cascade system, as demonstrated in Figure 4-3. The five-vane system allows the required rejection to be achieved, as computed using Fresnel's second order approximation of the Fresnel-Kirchhoff diffraction integral for a semi-infinite half-screen. The schematic plot on the right hand side of Figure 4-3 shows the nature of the function $\log(B/B_{\odot})$, where $B_{\odot}$ is the solar brightness, plotted with distance below the horizon. The heights and separations of the five vanes have been optimised to form an arc ensuring that the $(n+1)^{th}$ vane is in the shadow of the $(n-1)^{th}$ vane. The computed global rejection curve for this system is plotted in Figure 4-3 (bottom panel), together with measurements made using a full 5-vane mock up baffle in ambient and vacuum conditions which show good adherence to the predicted rejection levels.

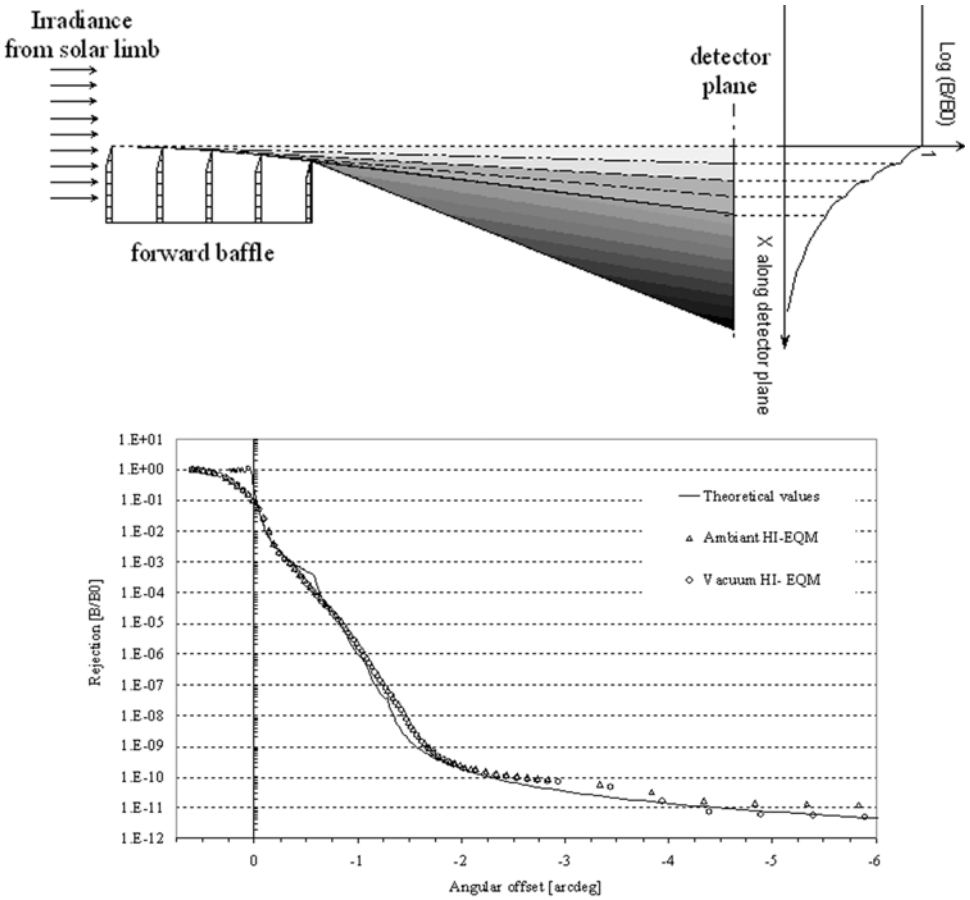

Figure 4-3 – The diffractive cascade knife-edge system of the forward baffle system

The relevant angular offset range for HI-1 for the test set-up recorded in the lower panel of Figure 4-3 is 1.5-3.3° providing a rejection of order 10^{-8} to 10^{-11} $B/B_{\odot}$. For HI-2 the rejection is of order 3×10^{-12}.

The perimeter baffle (lateral and rear side vane systems) protects the HI optical systems from reflection of photospheric light off spacecraft elements lying below the horizon defined by the baffles, including the High Gain Antenna, door mechanisms etc… However, one spacecraft element does rise above the baffles,

namely the 6 m long monopole antenna of the SWAVES instrument. Calculations show that scattered light from the monopole will be adequately trapped by the internal baffle system.

The internal baffle system consists of layers of vanes which attenuate unwanted light from multiple reflections into the HI-1 and HI-2 optical systems, mainly from stars, planets the Earth, zodiacal light and the SWAVES monopole. Although the Earth, stars and planets may be within the HI fields, the internal baffle system limits the uniform background scattered into the optical systems.

4.3 Optical Systems

Figure 4-1 shows the locations of the HI-1 and HI-2 optical units. The optical configurations for these are shown in Figure 4-4. These systems have been designed to cater for wide-angle optics, with 20° and 70o diameter fields of view, respectively, with good ghost rejection, using radiation tolerant glasses (as indicated by the notation for each lens), to cater for the deep space environment. The HI-1 lens system has a focal length of 78 mm and aperture of 16 mm and the HI-2 system has a 20 mm focal length and a 7 mm aperture. The design is optimised to minimise the RMS spot diameter and anticipates an extended thermal range from –20°C to +30°C. The detector system at the focus in each case is a 2048x2048 pixel 13.5 micron CCD.

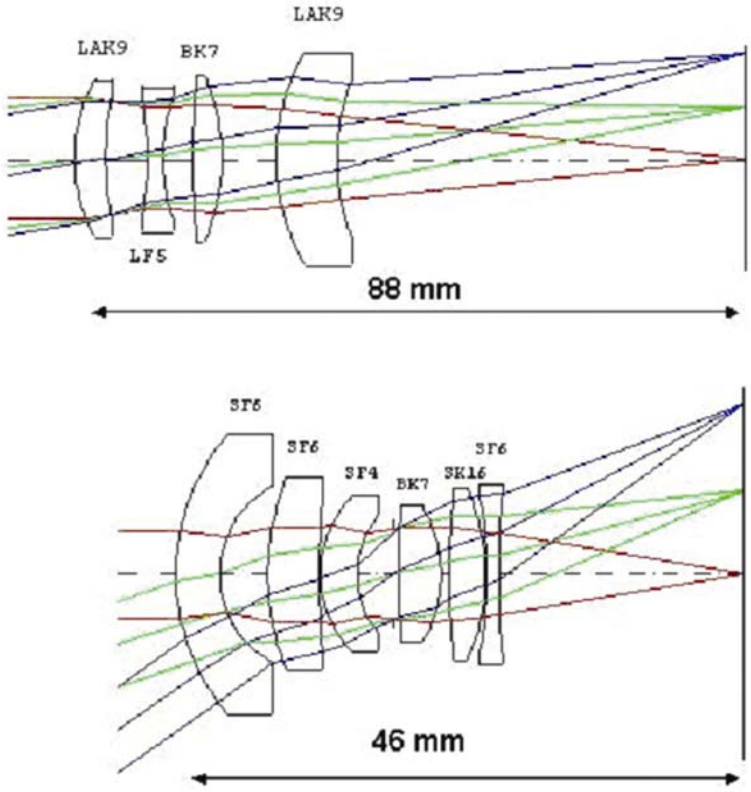

Figure 4-4 –[AV2] The optical configurations of the HI-1 (upper) and HI-2 (lower) lens barrels

The lens assemblies have undergone detailed design and test procedures and one of the key requirements is on the stray light rejection; the lens systems are mounted in blackened barrels. For HI-1 and HI-2 stray light rejection is measured to be at 10-3 or lower. This combined with the stray light measurement of the front

baffle, shown in Figure 4-4, provides an overall light rejection level of 10-11-10-14 for HI-1 and 3 x 10-15 for HI-2. These values are better than the straylight requirements (Table 1).

4.4 Instrument Performance and Contributions to the HI intensities

Table 4-2 summarizes the instrument efficiency, collecting area and other relevant parameters. The ultimate aim of this table is to estimate the intensity of the solar disc, for comparison to stellar, planetary and other sources. Knowing the mean photon energies of each system, and the size of the solar disc, one can calculate the solar intensity for HI-1 and HI-2 and the solar intensity per pixel.

Solar Constant [*C*] (mean value at 1 AU)	1372 Wm^{-2}
HI-1 collecting area (16 mm diam) [*A*]	2 x 10^{-4} m^2
HI-2 collecting area (7 mm diam) [*A*]	4 x 10^{-5} m^2
Detector Quantum Efficiency assumed [*DQE*]	0.8
Fraction of black body curve viewed [*bb*]	0.1 (HI-1) and 0.64 (HI-2)
Mean photon energy (HI-1) [*E*]	2.92 x 10^{-19} J (680 nm)
Mean photon energy (HI-2) [*E*]	3.31 x 10^{-19} J (600 nm)
Solar Image area (HI-1) [*pix*]	2076 (35 arcsec pixels, i.e. 2kx2k array)
Solar Image area (HI-2) [*pix*]	176 (2 arcmin pixels, i.e. 2kx2k array)
Solar Intensity (Bo) = [*C.A.DQE.bb/E]*	HI-1: 7.52 x 10^{16} photoelectrons.s^{-1} HI-2: 8.49 x 10^{16} photoelectrons.s^{-1}
Solar Intensity per pixel = [*C.A.DQE.bb/E.pix]*	HI-1: 3.63 x 10^{13} photoelectrons.s^{-1}.pix^{-1}. HI-2: 4.83 x 10^{14} photoelectrons.s^{-1}.pix^{-1}.

Table 4-2 – HI instrument efficiencies, collecting areas and intensities.

To assess the performance of the HI instrument, we consider briefly the intensity contributions of significant sources. This is described in detail by Harrison et al. (2005). Figure 4-6 shows a simulated image for HI-2 which includes all sources outlined below.

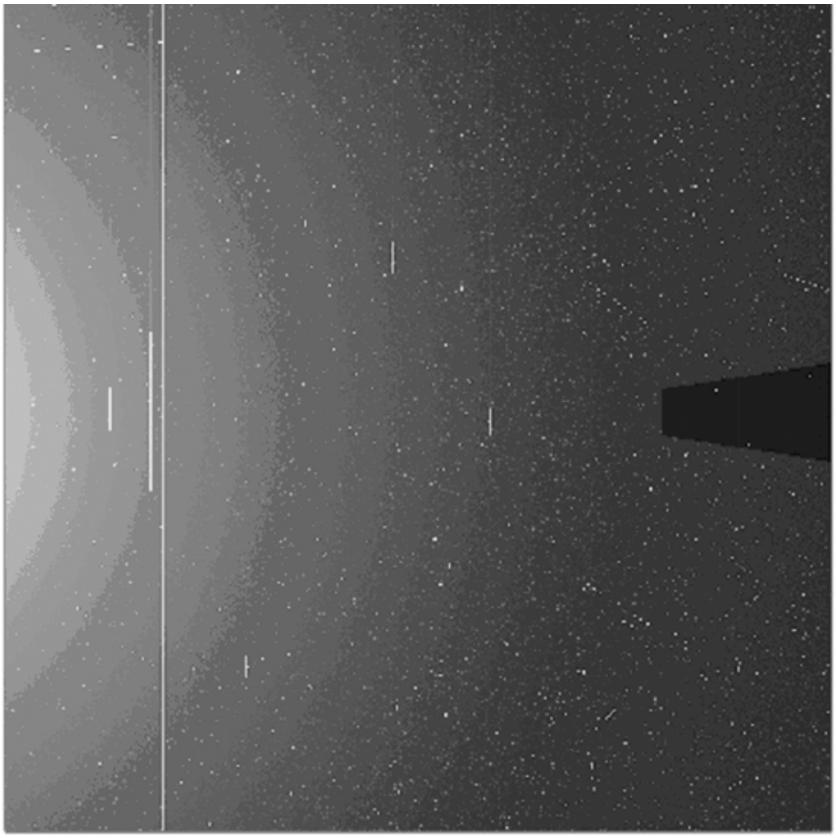

Figure 4-5 – A simulated HI-2 60 s exposure including all anticipated effects (see text). The Sun is to the left and the axis of the image running from left to right is the ecliptic plane.

Dust particles in the inner heliosphere form the so-called F-corona. The intensity of the F-corona is a function of elongation, the anticipated intensity distribution being given by Koutchmy and Lamy (1985).

Another major contribution to the HI images is the detection of planets. For the specific simulation we illustrate shown in Figure 4-6, the planets Mercury, Venus, Mars and Jupiter are included. These are the four brightest sources on the ecliptic plane (centre line). We have assumed that each planet is at its brightest magnitude. Having all major planets at their brightest intensity in one HI field would be rare; this extreme situation is used to simulate a worst case condition. The planetary and stellar magnitudes for this study are taken from Norton's Star Atlas (1998).

The planets, and, indeed, the stars, are point sources, which are added to the HI fields of view. Table 4-3 shows the maximum magnitude of the major planets and the brightness relative to the Sun, of the planets and some stars. To obtain the count-rate in photons per second for a point source in HI-1 or HI-2 we can compare to the Sun, using the figures from Table 4-2. The planetary intensities listed are the maximum intensities viewed from Earth. Since the STEREO spacecraft are in approximately 1 AU solar orbits, the same values apply.

The differences in the fraction of the black body curve detected by HI-1 and HI-2, combined with the different collecting areas, almost cancel out, resulting in very similar intensities in HI-1 and HI-2 for the planets and stars.

Object	Max Magnitude (m)	Brightness ($B = 10^{(-m/2.5)}$)	$B/B_{\odot}$ ($B_{\odot} = 5.25 \times 10^{10}$)	HI-1 Photoelectrons.s^{-1}	HI-2 Photoelectrons.s^{-1}
Sun	-26.8	5.25×10^{10}	1	8.46×10^{16}	9.55×10^{16}

Venus	-4.6	69.2	1.3×10^{-9}	1.10×10^{8}	1.24×10^{8}
Jupiter	-2.6	11	2.1×10^{-10}	1.78×10^{7}	2.00×10^{7}
Mercury	-1.8	5.2	9.9×10^{-11}	8.38×10^{6}	9.45×10^{6}
Mars	-1.6	4.4	8.4×10^{-11}	7.11×10^{6}	8.02×10^{6}
Sirius	-1.47	3.9	7.4×10^{-11}	6.26×10^{6}	7.07×10^{6}
Arcturus	-0.06	1.1	2.1×10^{-11}	1.78×10^{6}	2.00×10^{6}
Rigil	0	1	1.9×10^{-11}	1.61×10^{6}	1.81×10^{6}
Mag 1.0	1	0.4	7.6×10^{-12}	6.43×10^{5}	7.26×10^{5}
Mag 2.0	2	0.2	3.8×10^{-12}	3.21×10^{5}	3.63×10^{5}
Mag 3.0	3	0.06	1.1×10^{-12}	9.31×10^{4}	1.05×10^{5}
Mag 4.0	4	0.03	5.7×10^{-13}	4.82×10^{4}	5.44×10^{4}
Mag 5.0	5	0.01	1.9×10^{-13}	1.61×10^{4}	1.81×10^{4}
Mag 6.0	6	0.004	7.6×10^{-14}	6.43×10^{3}	7.27×10^{3}
Mag 7.0	7	0.0016	3.0×10^{-14}	2.54×10^{3}	2.87×10^{3}
Mag 8.0	8	0.00063	1.2×10^{-14}	1.02×10^{3}	1.15×10^{3}
Mag 9.0	9	0.00025	4.8×10^{-15}	4.06×10^{2}	4.59×10^{2}
Mag 10.0	10	0.00010	1.9×10^{-15}	1.61×10^{2}	1.82×10^{2}
Mag 11.0	11	0.00004	7.6×10^{-16}	6.43×10^{1}	7.27×10^{1}
Mag 12.0	12	0.000016	3.0×10^{-16}	2.54×10^{1}	2.87×10^{1}

Table 4-3 – Planetary and Stellar Intensities

Optical modeling shows that the HI-1 and HI-2 RMS size for a point source is of order 50 μm and 100 μm in the worst case, respectively. Note that the pixel size is 13.5 μm. Calculations show that of order 34 % of the spot energy is in the central pixel and this information, along with the RMS value, is used to model a basic Gaussian shaped point spread function (PSF). This is applied to all point sources in the simulation.

The straylight contribution can be calculated from the measurements given above and are included in Figure 4-5.

The stellar contribution is significant. The approximate number of stars per square degree, as a function of magnitude has been published (e.g. Allen, C.W., 2000) and we make use of this, projecting to the size of the HI fields of view. We do include a few stars of magnitude brighter than 0.0 in each calculation, which would be rather unusual, but is required to estimate the worst case situation. Thus, for the HI-2 simulation shown we assume the inclusion of Sirius, Arcturus and Rigil. We also assume that there is at least one star for each magnitude in the field of view. Table 4 shows the anticipated stellar distribution for the HI fields of view. Each star is added to the field of the modeled image at a location given by a random number generator. The PSF is applied to each star.

Mag	No. in HI-1 field	No. in HI-2 field
-1.47 (Sirius)	1	1
-0.06 (Arcturus)	1	1
0.0 (Rigil)	1	1
1.0	1	1
2.0	1	4
3.0	1	14

4.0	4	48
5.0	13	150
6.0	39	450
7.0	109	1335
8.0	314	3848
9.0	884	10843
10.0	2552	31277
11.0	6867	84156
12.0	18068	221414

Table 4-4 – Stellar numbers anticipated in the two HI fields of view for different magnitudes

To assess the performance of the HI we must include noise. For the simulation, a Poisson-like form is assumed. To do this, we modify the intensity of each pixel using a software function 'seeded' by a random number generator. This is a simple-minded yet effective approach for the purpose at hand. Noise is included in Figure 4-5.

The CCD pixels saturate at 200,000 photoelectrons. When a pixel saturates, the charge is 'spilled' or distributed along the column, rather than along rows (across columns). This saturation effect is called blooming. Cross-column saturation is subdued by the CCD design. The level to which saturation can be confined to columns has been confirmed with detector tests. Such confinement has been confirmed for pixel intensities brighter than the brightest values one would expect from Venus and Jupiter.

In Figure 4-5, this effect can be seen for the four planets and a few of the brightest stars. Note again, that having so many sources at that intensity in one field of view is extreme.

Another potential source of background is the CCD dark charge. However, at the design operating temperature of -70°C or lower the dark charge contribution is expected to be ~ 0.5 electrons.s^{-1} at the start of the mission. Even though this will increase with radiation damage it is still expected to remain small compared to the other sources of background signal.

The HI instrument does not have a shutter. The consequences of this are shown schematically in Figure 4-6. For the 2048x2048 CCD array, let us examine pixel (n,m) of an exposed image, and an exposure time of N seconds. The read-out direction of the CCD is downwards and the line transfer rate is approximately 2048 μs, resulting in a 'pseudo exposure' at every line position along the column under the pixel location. In other words in addition to the nominal exposure, there are (m minus 1) exposures of 2048 μs, which must be added to the nominal exposure intensity because there is no shutter.

In addition, the CCD is cleared using a 124 μs line transfer rate, so we must also add contributions from the (2048 minus m) pixels above the nominal location with an exposure of 124 μs at each location.

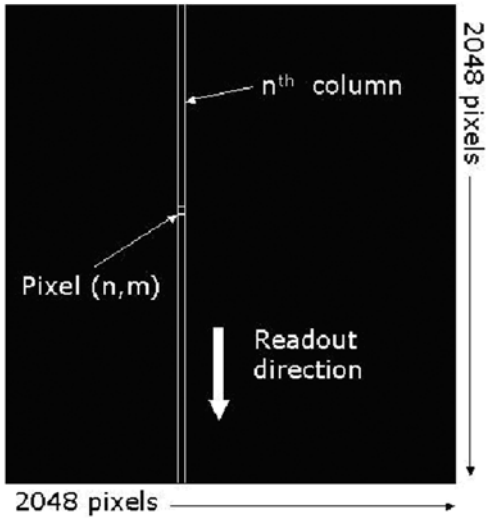

Figure 4-6 – A schematic of the non-shutter read-out

In mathematical form, the total count, *C*, for pixel (n,m) is given by:

$$C(n,m) = [Texp \times I(n,m)] + \Sigma(y=m+1,2047)\ (124 \times 10\text{-}6) \times I(n,y) + \Sigma(y=0,m-1)\ (2048 \times 10\text{-}6) \times I(n,y)$$

where the count rate for pixel (x,y) is given by I(x,y).

The effect is to introduce a background intensity gradient across the image readout direction, with step-function increases in this background in the columns below bright sources. The difference between the 60 s exposure and the 2048 μs 'exposures' for HI-2, for example, means that most stars produce an insignificant effect. In principle, the effect can be calculated and corrected.

Cosmic rays are added in random locations assuming a similar rate to those detected by the CDS instrument on the SOHO (Solar and Heliospheric Observatory) spacecraft (Pike and Harrison, 2000). Thus, we assume 4 hits.cm^{-2}s^{-1}. SOHO is located in an L1 orbit, 1.5 million km Sunward of the Earth, but the basic particle environment should be somewhat similar to that expected for STEREO. HI uses a 2048x2048 array of 13.5 micron pixels, i.e. 2.76 cm x 2.76 cm, which suggests 30.5 hits per second on each of the HI CCDs. In principle, cosmic ray hits can be point-like (single pixel), can spill into adjacent pixels or even be tracks. Thus, the simulated image of Figure 4-7 assumes cosmic rays incident from any direction.

To put the particle hit rate in perspective, note that for a 60 s exposure, we expect 1,830 pixel hits out of the 4,194,304 pixels, i.e. 0.04 % of pixels are affected. These will be cleaned on board before exposure summing. If such on board summing was not performed and accumulations of order 1 hour were required, we would expect 2.6 % of all pixels to be contaminated through cosmic ray hits.

Given all of the effects listed above, we have a requirement to extract the signal from a CME. The simulated image, in fact, includes a simple CME-like feature. It cannot be seen in the raw image. The CME is a simple, narrow loop set at an intensity of 10^{-15} Bo (see Figure 4-3). Given its location in the HI-2 field, this simulated CME is an order of magnitude weaker than anticipated events. To extract the CME signal we must accumulate exposures, to ensure that the CME intensity becomes significantly brighter than the noise level. As mentioned above, we do this by summing a series of exposures and cleaning each of cosmic rays, on board, prior to summing.

Once a summed image has been completed and downlinked, the CME signal is identified either by the subtraction of a base-frame (in which we estimate the F-coronal intensity) or the subtraction of a recent image. These approaches are in common use for coronagraph observations. A subtraction of a recent image

displays recent changes to the heliospheric brightness. However, if regular 'background' base-frames are calculated, from the anticipated coronal and other contributing intensities, we can provide regular monitoring of CMEs and a number of other phenomena. A simulated base-frame is extracted from the simulated HI-2 image to produce the image of Figure 4-7. This reveals the CME, which was not identifiable from the exposure in Figure 4-5.

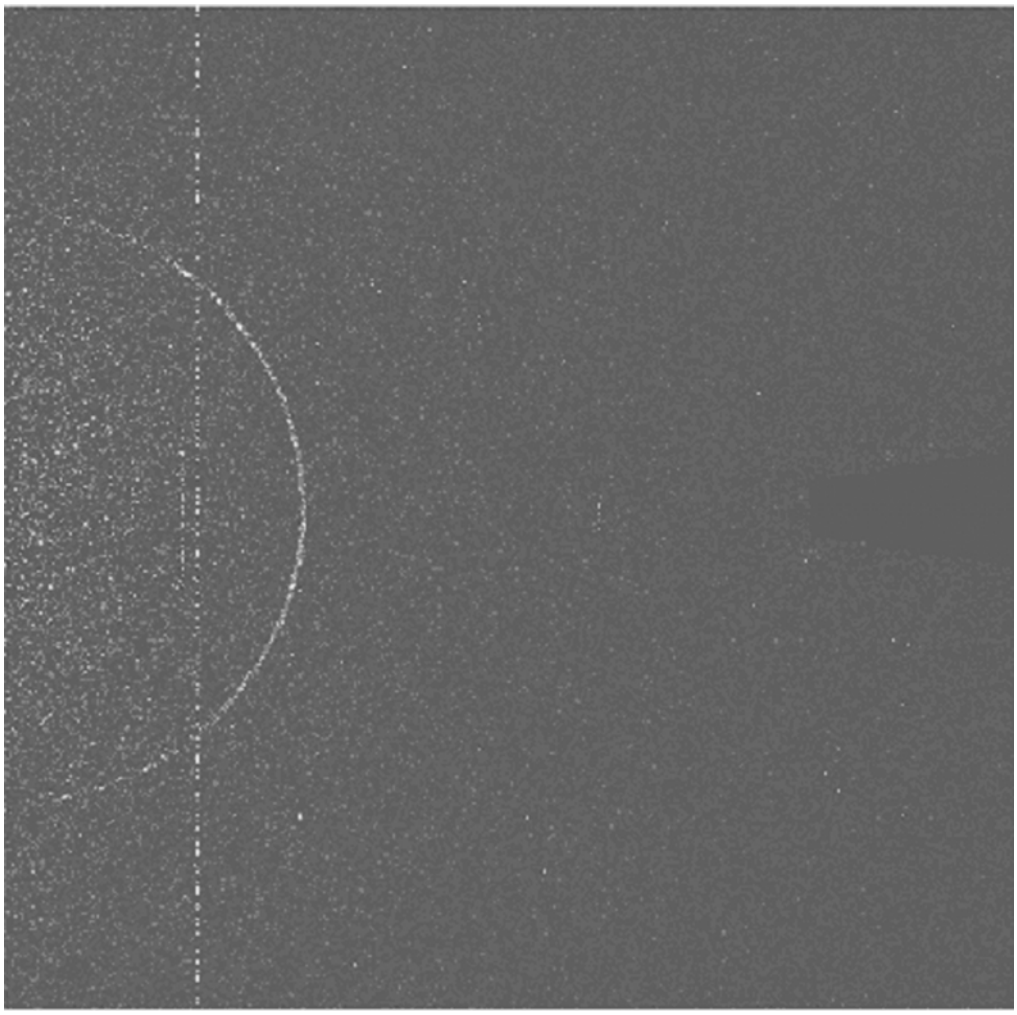

Figure 4-7 – A 60-exposue 60 s HI-2 sequence with the calculated base-frame subtracted. The CME loop is now identified.

This basic demonstration, utilizing all known effects in the HI exposures, and including extreme sources (bright planets and stars) and a weak CME, confirms that the HI performance is well able to be applied to the objectives set for the STEREO mission.

5. GUIDE TELESCOPE

The SECCHI Guide Telescope (GT) is an integral part of the Sun Centered Imaging Package and serves two main purposes:

1. The GT acts as the spacecraft fine sun sensor
2. The GT provides the error signal for the EUVI fine pointing system (FPS)

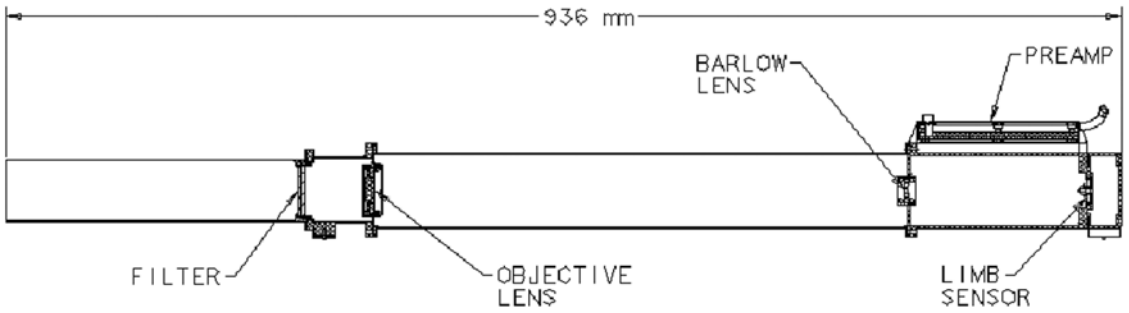

Figure 5-1. Schematic cross section of the SECCHI Guide Telescope

The SECCHI GT is based on the guide telescope for the TRACE explorer mission. The optics consist of an achromatic refractor with bandpass entrance filter and a Barlow lens (Figure 5-1). A set of 4 redundant photodiodes behind an occulter measure the location of the solar limb (Figure 5-2). The signals from the photodiodes are amplified and passed to the SECCHI Electronics Box. Table 5-1 lists key parameters of the GT. In contrast to the TRACE GT, the SECCHI GT has no provisions for off-pointing the GT relative to the science telescopes. The focal length of the GT for SECCHI is shorter than for TRACE, and is different for the Ahead and the Behind observatories. This extends the range of apparent solar diameters that the GT can accommodate, and allows the GT to operate throughout the elliptical orbit of each STEREO observatory. Figure 5-3 shows the two GT during their integration at LMSAL.

The analog photodiode signals from the GT pre-amplifier are sampled every 4 ms by a 12-bit analog-to-digital converter in the SECCHI Electronics Box. The SECCHI flight software converts the four diode voltages into pitch and yaw pointing error signals, and a set of four sun presence flags (one flag for each photodiode). Those signals are sent to the spacecraft. If all four photodiodes are illuminated, then the sun is within the linear range of the GT, all four sun presence flags are set, and the error signals are valid. If only one, two, or three photodiodes are illuminated, then the sun is within the acquisition range of the GT, and the STEREO spacecraft uses the sun presence flags to acquire the sun. The SECCHI flight software further processes the GT error signals to generate the drive voltages for the active secondary mirror of the EUVI Fine Pointing System.

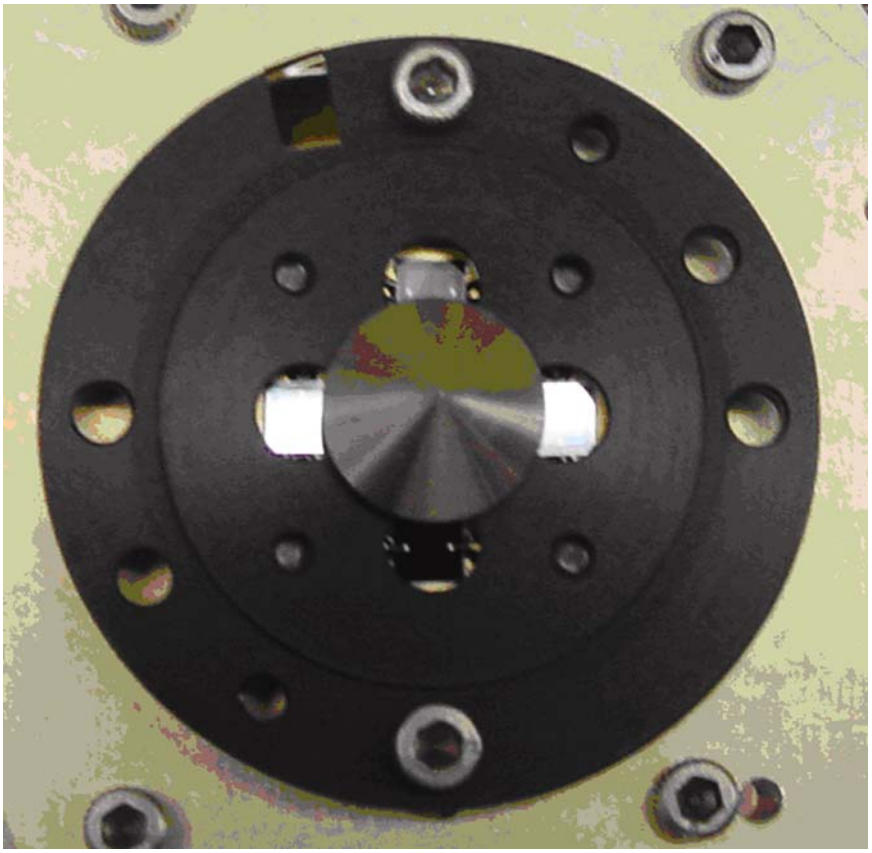

Figure 5-2. Guide Telescope sensor head with occulter and photodiodes.

Table 5-1 Key Guide Telescope parameters

Optics	Achromatic refractor with Barlow lens
Lens materials	Radiation hardened glass
Aperture	27 mm (aperture stop at objective lens)
Focal length	Ahead: 1454 mm, Behind: 1562mm
Bandpass filter	Center wavelength: 570 nm, bandwidth: 50 nm (FWHM)
Limb sensor	4 (+4 redundant) photodiodes
Telescope structure	Aluminum
Acquisition range	> ±20 arcmin (worst case)
Linear range	> ±70 arcsec (worst case Aphelion)
Pre-amplifier	Two selectable gains: sun / stimulus telescope (artificial sun)
Noise	< 0.4 arcsec (3σ, single sample)
Sample frequency	250 Hz (digital sampling in SEB)

6 SCIP BENCH

The SCIP structure supports the four SCIP telescopes (COR1, COR2, EUVI, and GT), the two SCIP electronics boxes (SCIP CEB and MEB), and the associated harnesses and thermal blankets. The design of the SCIP structure is driven by several requirements. The structure must (1) provide easy mounting and accessibility for component and spacecraft integration, (2) preserve the unobstructed field of view requirements of each telescope, (3) facilitate co-alignment activities and preserve telescope co-alignment on-orbit, (4) be sufficiently stiff to avoid coupling with spacecraft and launch vehicle modes, and (5) meet a stringent mass budget while surviving test and launch loads.

The SCIP structure is a simple optical bench. The four telescopes are mounted on one side of the bench while the electronics boxes are mounted on the opposite side. Several holes through the bench allow harnessing to pass between the telescopes and the electronics. The SCIP bench is a 2.5 inch thick aluminum honeycomb panel (44" x 27.25") with high modulus graphite/cyanate ester facesheets. Facesheet layup is biased for high shear stiffness and a resulting higher torsional stiffness of the optical bench. The design provides sufficient stiffness to meet the 50 Hz SCIP assembly first natural frequency requirement (measured a 54 Hz first mode, bench torsion, during assembly vibration testing).

An additional thermal tent structure is attached to the bench to support a "Quonset hut" of thermal blankets over the telescopes. The thermal tent structure is comprised of 1/4 inch honeycomb panels at the sun and anti-sun ends of the bench with tubular stringers connecting the panels. Thermal blankets are draped over the structure to control the thermal and contamination environments inside the Quonset hut.

6.1 SCIP Flexure Mounts

A key requirement of the SCIP structure is its ability to facilitate instrument co-alignment and maintain it throughout the test program and instrument life on-orbit. The key to meeting this challenging requirement is the development of a flexure-based near-kinematic mounting scheme. The scheme incorporates a set of three flexure mounts for each telescope. Each mount is very stiff in the normal and lateral directions and much less stiff in the axial direction and in the three directions of rotation. Acting as a set of three, the mounts provide a fully constrained, but not over-constrained, mounting scheme. The design of the flexure mounts has several distinct advantages: (1) The ratio of modulus in the "stiff" directions to the modulus in the "released" degrees of freedom provides an essentially kinematic mounting system. (2) The kinematic nature of the mounts minimizes thermal stress in the telescopes, preserves co-alignment on-orbit and allows shimming of the telescopes without inducing stress in the telescope tube structure. Shimming of the telescopes was performed with 5 arcsec resolution. (3) The mounts utilize snug fitting pins at each interface to prevent shifts after integration and assure co-alignment repeatability when a telescope is removed and reinstalled. (4) The titanium alloy provides high strength and stiffness with low mass, and large thermal isolation.

6.2 Analysis and Testing

The primary analysis tool for the SCIP structure was a MSC/NASTRAN finite element model. The SCIP optical bench was modeled in detail, including models of each telescope and of the electronics box, with a 189,000 degree of freedom model. Due to the developmental effort on the flexure mounts, a highly detailed (140,000 degree of freedom) model was constructed to analyze high stress areas and predict mount stiffness. Based on the detailed model, a simplified model of the mount was constructed for use in the assembly-level model. The full assembly-level model was used to predict assembly first frequency, assess stress levels in the structure, derive component test spectrums and interface loads, and predict on-orbit telescope alignment shifts due to thermal loads.

Significant testing was performed to correlate the finite element results and load test the flight structures. The flexure mounts went through two rounds of prototype testing before the flight design was finalized. A monolithic telescope simulator facilitated testing of the mount system to determine its mounting stiffness. After the flight hardware was manufactured, other simulators were constructed to be used in static and

dynamic load testing of the flight article. The test results were used to validate the component test spectra that were used to qualify the telescopes before they were integrated with the flight optical bench.

7 MECHANISMS

The SECCHI SCIP telescope suite contains a total of 10 mechanisms of 6 distinct designs. EUVI has a focal plane shutter, filter wheel, and a quadrant selector. The COR-1 and COR2 telescopes each have a focal plane shutter and polarizer mechanism. All three of the SCIP telescopes have a door mechanism. The HI telescopes have one mechanism, a door, which was discussed in Section 4.

All mechanisms have heritage from previous flight programs. The SCIP door mechanisms are based on a SOHO-LASCO design. The EUVI quadrant selector is an evolution from the mechanism used in the TRACE quadrant selector, in that there are no restrictions in the frequency of changes between telescope quadrants. The EUVI filter wheel, CORx polarizer wheels and shutter mechanisms are nearly identical to the ones used on GOES SXI-N.

7.1 SCIP Aperture Doors

The re-closable doors of the EUVI, COR1 and COR2 telescopes comprising the Sun Centered Imaging Package (SCIP) are referred to as the SESAMEs - the SECCHI Experiment Sun Aperture MEchanisms. In total there are two sets of SESAMEs, one for each SCIP assembly. The prime objectives of the re-closable doors are to protect the sensitive optics of the telescopes from damage due to contamination during ground operations, but also at critical times during flight operations. The launch of the Delta rocket generates large acoustic vibrations requiring the door lids to be pressed tightly against the telescope entrance apertures without generating particles. The EUVI is especially sensitive because the lid has to protect the thin optical filters lying directly behind it. The doors also help to maintain the cleanliness of the optical systems from external contaminants, especially CORx, that may be caused during thruster firings to control the orbit of the STEREO spacecraft. Because of momentum desaturation the thrusters will be fired about every 6 days on average, implying that the COR doors will be cycled about 120 times during the two-year nominal operations period. Re-closable doors are also required because the optical systems must open and close during ground testing and calibration of the optical systems.

All three doors have a similar baseline design. They are all operated by a stepper motor which drives a special screw-ball bearing mechanism to open and close the lids. In case of the malfunction of the motor a paraffin actuator acts as the failsafe device to open the door permanently. The command to "fire" the paraffin actuation is controlled by the spacecraft. The doors can be driven by the motors into different positions: superclosed, closed, cracked and open. The superclosed position presses the door lid against the aperture to withstand the launch environment, which could cause the lid to vibrate against the box. This vibration would create particles. The closed position is the normal closed position without the launch pre-load. The cracked position is an intermediate position between closed and open to permit outgassing to occur after launch. The open position is the normal position for science operations. The lid designs of EUVI and CORx have different sizes and structures, with calibration windows being integrated into the COR lids. The opening angle of the EUVI door is 90°, that of the COR doors is 270°.

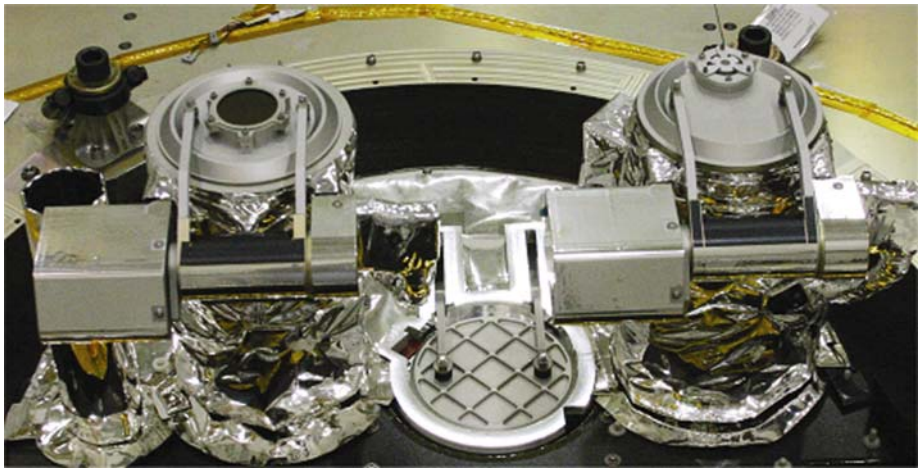

Figure 7-1. Top front view onto the SCIP-B assembly after integration into observatory B. From left to right: COR 1, EUVI and COR 2 doors. The SCIP-A doors are identical.

7.2 Shutters

The EUVI and CORx shutter designs are based on shutters that have successfully flown on SOHO/MDI and TRACE and will be flown on GOES-N/SXI and Solar-B/FPP. Both consist of a brushless DC motor with an optical encoder to which is attached a thin circular blade with a 120° opening that is positioned in front of the telescope's focal plane. The motor rotates the blade to open the shutter, exposing the CCD. The blade is rotated in the same direction to close the shutter. The SECCHI shutters are capable of exposures from 40 ms to 67 seconds in a programmable mode that are repeatable to better than 15 μsec and uniform across the CCD to 50 μsec. The exposure length can be indefinite when open and close motions are controlled directly by the SEB.

7.3 Quadrant Selector

The EUVI quadrant selector is nearly identical in design to the coronagraph shutters. The motor rotates a blade with a 90° opening just behind the telescope's thin-film entrance filters. The mechanism is commanded to rotate in 90° increments in approximately 45 ms to mask off all but one of the telescope's four EUV channels. Table 1 shows the mapping of the quadrant selectors target positions to the telescope channels.

Table 1		
Telescope Channel	**CW Target**	**CCW Target**
17.1 nm	20	23
28.4 nm	14	17
19.5 nm	8	11
30.4 nm	2	5

Table 2			
Filter Configuration	**Position Name**	**CW Target**	**CCW Target**
Single Filter	S1	22	23
Double Filter	DBL	67	68
Single Filter	S2	112	113
No Filter	OPEN	157	158

7.4 EUVI Filter Wheel

EUVI also incorporates a four position filter wheel just behind the telescope's shutter. The filter wheel consists of a 101 mm diameter brushless DC motor surrounding a rotor with four 32 mm diameter through holes. Two of these holes contain a single layer thin-film aluminum filter on nickel mesh similar to the entrance filters. Another contains two of the same filters in series to provide redundant visible light blocking should the entrance filters at the front of the telescope fail or degrade. The final position is left open. The mechanism will be launched with the filter wheel in this position, leaving the telescope beam-

path open and protecting the three-filter position within the mechanism housing. Operation time between two adjacent filter positions is approximately 300 ms. Like the SECCHI shutters, the filter wheel has heritage from TRACE, MDI, SXI, and FPP. Table 2 shows the mapping of the filter target positions to the filter configurations.

7.5 Polarizer Wheel

The coronagraph polarizer mechanism, also known as the hollow-core motor (HCM), is the most unique of the SECCHI mechanisms. Its design is derived from a similar mechanism used with success in MDI. It has a 144 step brushless DC motor similar to that used for the EUVI filter wheel. A large-diameter, thin-section bearing supports a stainless steel rotor with Teflon toroid separators. The space inside the bearing is left open, providing a 48 mm clear aperture for the coronagraph light bundle. With the 144 step motor design, the polarizing optic that is mounted to the rotor can be positioned in 2.5° increments. During normal observing operations, the polarizer mechanism will rotate 120° with an angular repeatability of better than 30 arcseconds. It makes this move in approximately 400 ms.

7.6 Lifetime Requirements

The lifetime requirements for each of the SECCHI mechanisms are 2.1 million operations for the EUVI quadrant selector, filter wheel, and shutter and 0.6 million operations for CORx polarizer mechanism and shutter. Comprehensive life testing was completed to prove the designs of the EUVI quadrant selector, coronagraph shutter, and HCM. These mechanisms underwent vibration to levels greater that that for flight, thermal functional testing, and flight like operation in vacuum to three times their design lifetime. The quadrant selector was qualified to 8 million operations, the coronagraph shutter qualified to 2.8 million operations, and the polarizer mechanism qualified to 3.5 million operations with no degradation in performance. The designs for the EUVI filter wheel and shutter were previously proven to be capable of more than 32 million operations.

8 SECCHI Electronics

SECCHI contains three types of electronics arranged into 4 different boxes. The main electronics is contained within the SECCHI electronics box (SEB) and is described in Section 8.1. The SCIP mechanisms are driven from a remote electronics box, described in Section 8.2. The SCIP and HI cameras are driven from remote electronics boxes, called the Camera Electronics Box (CEB) and described in Section 9.

8.1 The SECCHI electronics box (SEB)

The SEB (SECCHI Electronics Box) is the payload controller for the SECCHI Instrument Package on the STEREO spacecraft, controlling and monitoring all SECCHI hardware. The SEB provides the instrument's interface to the spacecraft via the MIL-STD-1553 and power interfaces. It receives and distributes commands from the spacecraft and collects and converts state of health telemetry data before providing it to the spacecraft. Image data from the telescopes (2 channels, 100MB/s) is received over two spacewire ports and is then processed, compressed, and transmitted across the 1553 interface to the spacecraft for downlink. The SEB had to be designed to meet stringent program EMI requirements, as will be discussed briefly below. An EDM was designed and built before the flight hardware as a pathfinder for the designs. This EDM is now part of the software testbed that will be maintained during the life of the mission. The flight hardware underwent EMI/EMC, vibration and thermal-vacuum testing before integration with the SECCHI instrument packages.

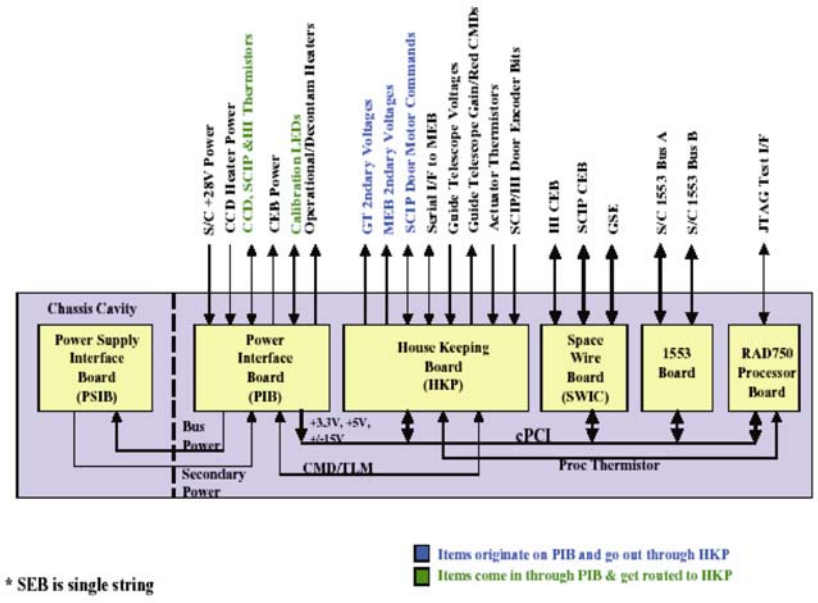

FIGURE 8-1 SECCHI Electronics Box (SEB) Functional Block Diagram

8.1.1 Enclosure

The enclosure was machined from a single block of aluminum. It includes 2 compartments allowing EMI isolation of the internal DC/DC converters. The bottom and one side have removable covers with labyrinth seals. Individual cards are installed from the top, with each card having a connector bracket that provides additional EMI protection and structural tie points. One final top cover, with clearance for each connector, completes the EMI seal. The DC/DC converters reside in a separate "EMI cavity" isolated from the main cavity. The interface between the 2 cavities is achieved with an EMI-tight, filter capacitor panel. The overall dimensions are 7.8in x 11.5in x 10.5in (H x W x L), weighing 9.4kg (20.7lbs).

8.1.2 Motherboard

The SEB Motherboard provides electrical connectivity between all cards housed within the SEB enclosure. It is a customized, cPCI compliant, five (5) slot, 6U back plane. The first four (4) cPCI slots which utilize the PCI signaling strictly adhere to the cPCI specification. The fifth slot which does not use the PCI signaling has been customized for communications on the user defined connectors, P3/P4/P5. Unused cPCI connectors were eliminated from the design.

8.1.3 Electrical Power

The SEB must interface to the spacecraft's unregulated power bus. The electrical power system provides this interface as well as power conversion, control and distribution. Due to EMI requirements, the electrical power system was divided into two (2) functional assemblies – the DC/DC converters and related circuitry (PSIB) and the power interface and distribution functions (PIB).

The PIB interfaces to the primary spacecraft power bus through a front panel connector and routes this power off the motherboard and through the EMI cavity line filter panel, to the DC/DC converters in the small EMI cavity. Regulated secondary power is then routed back from the DC/DC converters to be distributed throughout the SEB and SECCHI system by the PIB card. Internal secondary SEB power is distributed across the motherboard as required. External SECCHI power is routed through PIB I/O connectors and, in some cases, across the motherboard and out through the HKP I/O connectors due to front panel limitations. Power control signals are generated from gate arrays resident on the HKP card, as commanded by the RAD750 processor card. The HKP card determines the proper commands to send to the PIB and uses a serial interface across the motherboard to transfer the information. The PIB also provides motor drive power from control signals generated on the HKP. Voltage and current monitoring circuits on board provide state of health telemetry to the HKP for conversion and, ultimately, downlinking. This card also houses the operational heater drive circuits with appropriate switching for thermal control of the instrument package. The heaters are again controlled via the HKP card since the PIB has no interfaces with the processor for real estate and design simplification reasons. A second power bus from the spacecraft is distributed to SECCHI decontamination heaters through latching relays on this card.

The PSIB assembly resides in the small EMI cavity and includes three (3) DC/DC converters that provide all secondary power for the SEB and SECCHI system, as well as all necessary filtering and protection. A single converter provides +3.3Vdc power for internal logic. A triple output converter provides +5VDC for internal and external legacy logic and +/-15Vdc power for analog functions. The third converter provides +15Vdc dedicated for "noisy" motors and mechanisms. Primary and secondary power interfaces, to the main cavity, are through an EMI filter panel.

8.1.4 RAD750 Processor

The SEB RAD750 processor, procured from BAE Systems, provides all processing required for the SECCHI system and the control of all SEB circuitry via the cPCI backplane. At the core is a custom Power PCI Bridge chip providing the interface between the PowerPC 750 and the cPCI bus. The primary computing resource is the radiation hardened PowerPC 750. The RAD750 card provides for 256kbytes of EEPROM StartUp ROM (SUROM) and 128Mbytes of SDRAM. SDRAM EDAC can correct nibble errors and detect double nibble errors. The card provides a self-refresh mode and scrubbing for the SDRAM. The RAD750 is capable of 120MIPS and is being run at 116Mhz in the SECCHI application. This card is the only 3U card in the SEB.

8.1.5 MIL-STD-1553 Interface Card (1553)

The 1553 card provides a fully compliant MIL-STD-1553 Remote Terminal (RT) bus interface to the spacecraft and 3Mbytes of EEPROM storage for software application code. The 1553 interface is the only communications interface with the host spacecraft. All commands, data uploads and telemetry are communicated across this bus. Full redundancy makes this a very robust interface. The EEPROM is arranged as two (2) banks of 1.5Mbytes X 16bits wide. This storage is fully accessible across the cPCI bus and provides for redundant flight software storage.

8.1.6 SpaceWire Interface Card (SWIC)

The SWIC provides two (2) 100Mb/s, simultaneous SpaceWire compatible links to the SCIP and HI instruments respectively. All image data and camera setup commands are transferred using these interfaces. The TSS901E ASIC, from Atmel, provides these SpaceWire links. 256Mbytes of SDRAM allows for temporary image storage while awaiting retrieval and processing by the RAD750, and can also be used by the processor for data storage or program execution. The SDRAM is complete with programmable refresh, scrubbing and EDAC. To efficiently move large amounts data, the PCI interface can be configured for DMA transfers, on to or off of the SWIC.

8.1.7 Housekeeping Card (HKP)

The HKP is the bridge between the analog interfaces and the digital cPCI bus for the SEB. It controls serial data transfers with the SCIP mechanisms controller (Mechanisms Electronics Box – MEB hardware) for shutter control and other commands. All SECCHI door status is monitored and made available by the HKP. A regulated current source provides selectable drive for SECCHI calibration LED illumination. Analog Guide Telescope signals are received and digitized by the HKP at a 250Hz rate for delivery to the processor for transfer to the spacecraft's Attitude Control System (ACS). Sixty three analog telemetry points, including voltage, current and temperature sensors, for both SEB internal and SECCHI external, are digitized (0 to +10V range, 12 bit conversions) and made available to the system processor for use in fault detection and isolation and general state of health monitoring.

8.2 Mechanism Electronics Box (MEB)

All of the SECCHI SCIP mechanisms, with the exception of the telescope doors, are controlled by the SECCHI Mechanisms Electronics Box (MEB), which is mounted on the underside of the SCIP optical bench. Physically, the MEB is a 210 × 56 × 171 mm box with a mass of approximately 1.4 kg with connectors dedicated to power and commands from the SEB and each of the telescopes. The MEB inputs are a Low-Voltage Differential Signal (LVDS) from the SECCHI SEB, 5V power for the MEB and mechanism encoders, ±15V power to drive mechanism motors. The three LVDS inputs to the MEB from the SEB include a strobe, clock signal, and a serial command signal. A single return LVDS signal is sent back to the SEB. The MEB contains two boards and each has two Field Programmable Gate Arrays (FPGAs). The FPGAs on the first board control the EUVI shutter, quadrant selector, and filterwheel, and drive the EUVI Fine Pointing System (FPS). The two FPGAs on the second board each control a shutter and polarizer mechanism on one of the coronagraphs.

The MEB accepts low level commands such as "load target position," "move clockwise" to that position, and "read current encoder position." These commands are sequenced by the SEB and there is no command buffer in the MEB. Table 8-1 provides a partial listing of commands accepted by the MEB in the order in which they are typically employed. MEB commands are 16-bit and consist of an 8-bit command word and an 8-bit variable word such as exposure time for a shutter or target position for the HCM.

Table 8-1. MEB Commands

Command	Action
RESET	– HCM and filter wheel target and encoder reading cleared – Shutters rotate to "ready for exposure" position, exposure time cleared – Quadrant selector rotates to 284Å quadrant, target cleared
LOAD TARGET	HCM, filter wheel, and quadrant selector desired position saved
MOVE CW	Mechanism moves to saved target
LOAD EXPOSURE	Shutter desired exposure time saved
CW EXPOSURE	Shutter makes a 120° clockwise move to open position, waits for desired saved exposure time, and makes a 240° clockwise move to closed / ready position
READ ENCODER	MEB returns to the SEB the current position of the mechanism
READ STATUS	MEB returns to the SEB the current status of the mechanism

The mechanism motors are driven by a 15V, three-phase signal generated by the MEB in response to the signal provided by the optical encoders in each of the SECCHI mechanisms. The SECCHI MEB also drives the EUVI FPS, the design of which is discussed in a separate section. The MEB accepts commands from

the SECCHI SEB to derive three analog voltages from 0-10V to drive the ISS PZTs. There is no PZT or mirror position feedback to the MEB.

9 Charge Coupled Device (CCD) Cameras

9.1 CCD Detectors

All 5 telescopes use the same CCD architecture. The CCDs are E2V (formerly Marconi and EEV) CCD42-40s with 2k x 2k pixels of 13.5 μm pitch. The CCDs are thinned, back-illuminated, and operate non-inverted to ensure good full well capacity (150k to 200k electrons). The standard product has a single serial shift register with an output node at each end of the register. However to save mass only one output node is enabled in flight. The COR1, COR2, and HI instruments are fitted with standard anti-reflection coated chips (optimized for the 450-750 nm range). The EUVI has a bare (non-coated) device optimized for the EUV range (15-30 nm).

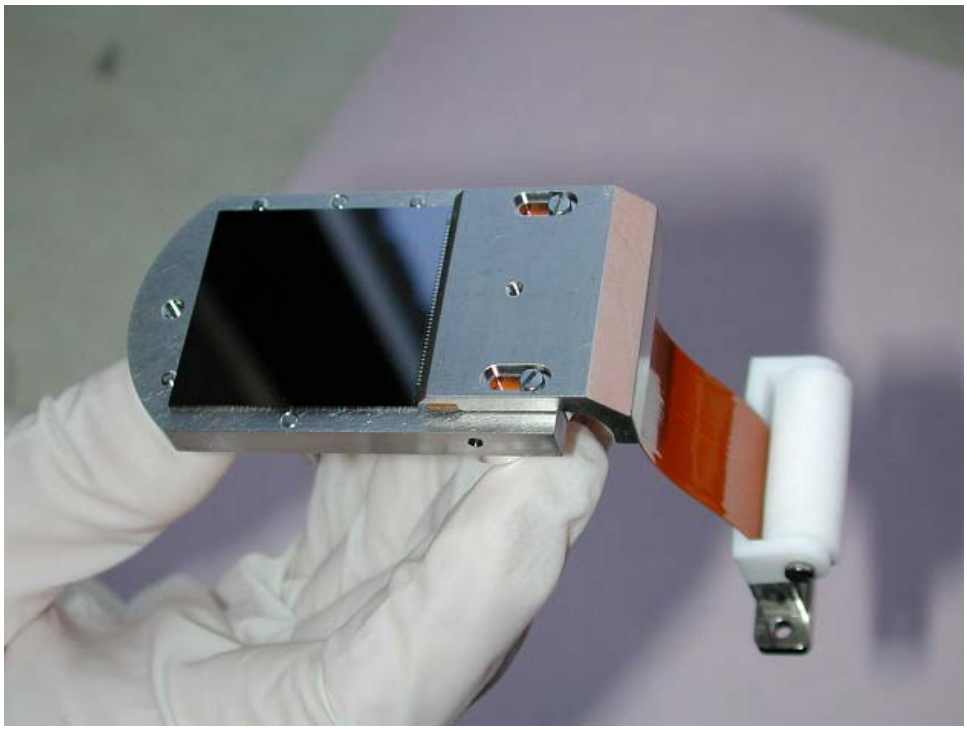

Figure 9-1. SECCHI CCD in its package, with flexprint harness attached. The size of the CCD is about 28.1 mm x 30.3 mm.

9.2 Focal Plane Assembly (FPA)

The CCDs are mounted into a focal plane assembly that was design by NRL/Swales and manufactured at the University of Birmingham. The original plan was that the mechanical design of the FPA would be the same for all 5 telescope applications. However, this was not possible and only COR1 and COR2 had the exactly the same design and the other 3 telescopes used similar concepts, but were different designs.

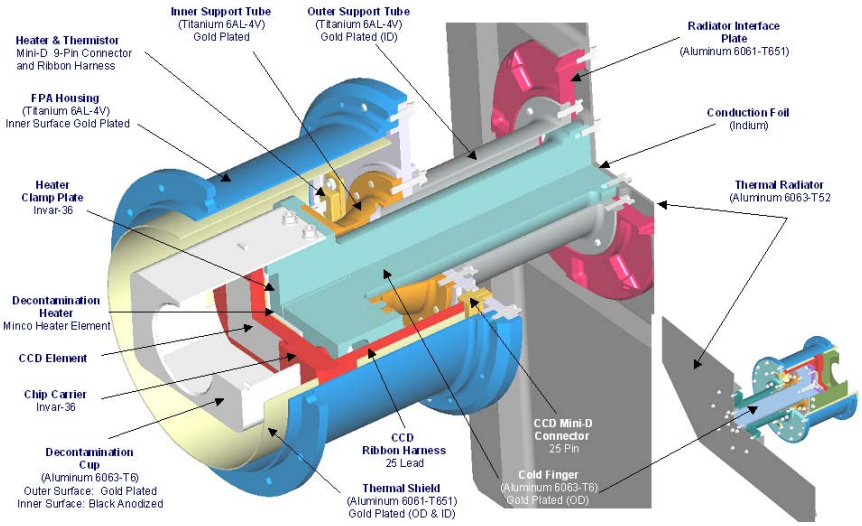

Figure 9-2. COR FPA

The requirements for the design of the FPA were (1) Cool the CCD using passive radiation techniques to –80C using an aluminum cold finger coupled to a surface radiating to deep space; (2) Position the CCD at the focal plane of the telescope, perpendicular to the optical axis and aligned to the optical axis; (3) Keep the CCD positioned at room and operating temperatures. (4) Keep motions of the focal plane to be repeatable (5) Provide a capability to add a spacer in between the FPA and telescope mounting flange; (6) Provide a capability to heat the CCD to at least 40 C to drive off contaminants and to "anneal" the CCD after radiation damage; (7) Provide a cold cup at a temperature slightly colder than the CCD to act as a contamination shield for the CCD

9.3 Camera Electronics Box (CEB)

Figure 9-3 is a schematic of the SECCHI CCD camera system, comprising the SECCHI Electronics Box (SEB), and two Camera Electronics Boxes (CEBs): one for the SCIP, and one for the HI.

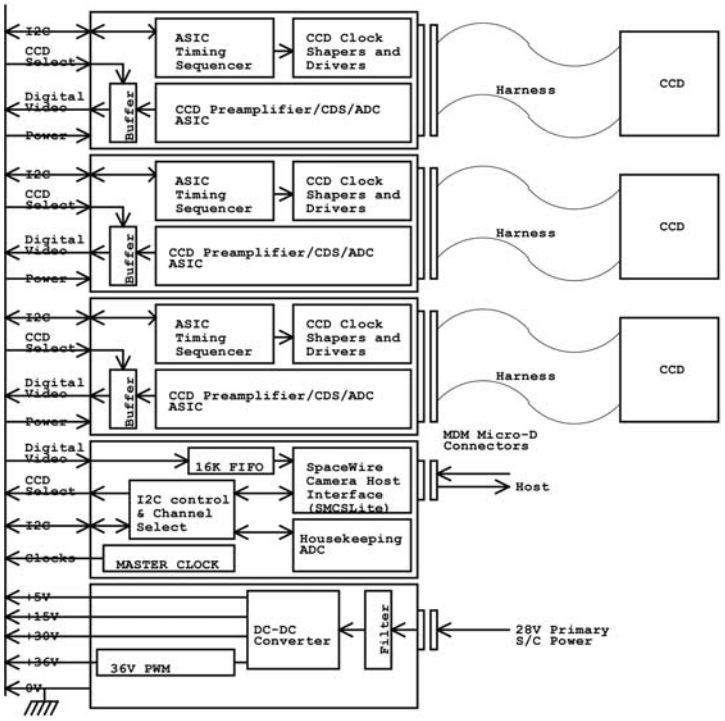

Figure 9-3. CEB Architecture.

Figure 9-4 is a schematic of the CCD Camera Electronics Box (CEB). It comprises

- Two (HI) or three (SCIP) CCD Driver Cards; one dedicated to each of the CCDs. A block diagram of the CCD Driver Card is shown in Figure 9-4.
- A Camera Interface Card that provides a common interface between the three CCD Driver Cards and the SECCHI instrument computer.
- A DC-DC Power Converter mounted in an internal screened housing in the base of the electronics box.
- A backplane interface for inter-connection of the daughter PCBs.

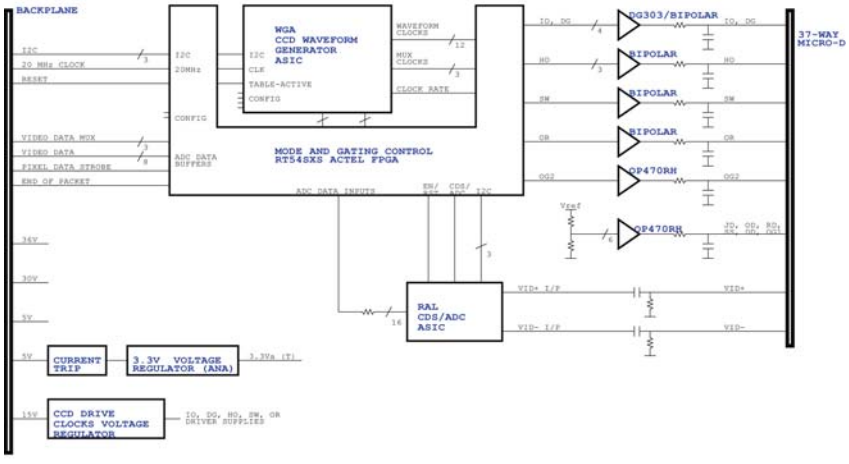

Figure 9-4. CCD Driver Card.

Each CCD Driver Card (Figure 9-4) accommodates a dedicated waveform generator and sequencer ASIC, CCD clock drivers, low noise DC bias supply generators, a CCD video preamplifier, correlated double sampler (CDS), and 14 bit analogue to digital converter (ADC) system.

The requirement specification for the STEREO/SECCHI CCD camera controllers calls for a CCD pixel readout rate of 1 Mpixels/s, yet also dictates very challenging low mass and low power budgets. ASIC and surface-mount packaging technologies help minimize the size, mass, and power requirements of the cameras. Controlling three CCDs from the SCIP box, and two CCDs from the HI box minimizes the overheads arising from the spacecraft interfaces and the power converters, and thus the overall size, mass, and power of the camera controllers.

The camera electronics exploits the same basic waveform generator ASIC and CCD clock driver circuit topologies designed for the SMEI CCD cameras, but updated for faster pixel readout rate for SECCHI. Each CCD is clocked from its own dedicated sequencer and clock drivers, and is read out through its own 14 bit CDS/ADC video processor.

The 14 bit CDS/ADC video processor is implemented in an ASIC which is a purpose-designed, radiation tolerant chip under development at RAL.

Each camera communicates with the SECCHI instrument computer via an IEEE1355/SpaceWire link, enabling camera programming, camera command, gathering of housekeeping data, and the transmission of digitised CCD video data. The data transmission rate is up to 100 Mbits/s, employing the SpaceWire LVDS hardware interface standard. Exposure timing for each CCD is controlled directly from the SECCHI instrument computer. Appropriate programming and control of the camera waveform generator ASICs enables updating of CCD readout waveform patterns and readout tables, and the initiation of various readout modes e.g. clearing, exposure, full-frame, windowed, or continuous readout. Pixel binning, programmable video gain, and programmable video DC offset level are also supported.

Each camera contains a DC-DC power converter that converts the incoming 28 V spacecraft primary power to the required +5 V, +15 V, +30 V, and +36 V secondary supplies. The camera's 28 V power supply input is in-rush current limited, and current-trip protected. The converter's output supply rails are also filtered to minimise any noise and/or current-switching transitions on the supply rails to the CCD drive circuitry. The complete power converter system is screened from the CCD drive electronics within its own shielded sub-housing within the Camera Electronics Box.

The survival power and decontamination heater power supplies for the CCDs are not routed through the camera boxes, but go directly from the SECCHI instrument computer to the CCD heads. Similarly, the temperatures of the CCDs are monitored directly from the SECCHI instrument computer and not through the camera electronics units. Housekeeping telemetry from the camera electronics enables the controller's secondary power supply voltage rails and internal temperature to be monitored.

The SCIP camera electronics enclosure is 195 mm x 126 mm x 85 mm, including all mounting feet, connector, and fixing screw protrusions. The HI camera electronics enclosure is slightly smaller (195 mm x 126 mm x 70 mm) to conserve volume and mass. The wall thickness is 2.0 mm, and the internal pitch between PCBs is will be 13.716 mm.

Operationally, the camera will respond to the following modes:

Clear

Clearing of the CCD will take advantage of the CCD's 'dump-drain' running adjacent to the serial output register. Appropriate programming of the ASIC waveform generator will allow the entire array to be cleared any number of times prior to integration.

Integration

During integration, the CCD's parallel register clocks will be held at appropriate voltage levels. The serial register clocks can be individually programmed to be high, low, or clocking. Dither clocking of the parallel register clocks will be possible to help minimise dark current generation, and to allow some degree of testing at room temperature.

Readout

Appropriate programming of the ASIC waveform generator will allow any number of readout modes including:

(1) full-frame readout of n lines,
(2) windowed readout of at least two windows (dump n lines, read x lines, dump m lines, read y lines, etc),
(3) full-frame, or windowed readout with n x m pixel binning (pixel binning parameters can be different between windows provided that the windows are not overlapping),
(4) Continuous clocking.

The size of the readout area (or image format) is programmable without restrictions. Multiple windowed readout is possible up to the memory limits of the ASIC's internal 'readout table' memory. Window co-ordinates are programmable within CCD 'readout tables', but must be specified from the control computer. Any variety of camera operating cycles will be possible by appropriate programming of the waveform generator ASIC. Cycles may be implemented as a series of short 'readout tables', individually initiated from the control computer; or alternatively as one long 'readout table' initiated only at the beginning.

10 Flight Software

The SECCHI flight software is a real-time multi-tasking VxWorks software that provides all of the software services needed by the instruments. This includes handling commands from the spacecraft, housekeeping and science telemetry to the spacecraft, heater control, guide telescope control, instrument control, image scheduling and image processing. The code is derived from spacecraft code used in NASA's Small Explorer (SMEX) series of satellites, which was then modified for the SECCHI instrument.

The VxWorks operating system provides the infrastructure for running multiple tasks and each of the major functions listed above are run as separate tasks that can be started, stopped or reloaded independently. This made modifying the original SMEX code easy since the code is naturally modular. VxWorks also provides inter-task communications, which have been developed into a software bus library, shared by all tasks. The heritage software provided a large amount of useful code which reduced our task to modifying the telemetry and command tasks for SECCHI hardware and STEREO spacecraft protocols, developing new tables, telemetry and commands within the SMEX framework and developing new SECCHI code for image scheduling, image processing and control of the SECCHI hardware, specifically cameras, mechanisms, heaters, power, housekeeping board. The SECCHI flight software contains about 250,000 lines of code.

10.1 Instrument Scheduling

The STEREO spacecraft will use the NASA Deep Space Missions System for commanding and telemetry downlink. Only one or two 4-hour contacts per day per spacecraft are planned. During the contact time the uplink rate is 2 kbits/sec shared between all instruments and the spacecraft, which means limited daily commanding and a need for handling large blocks of schedule. The distance of the spacecraft from Earth and the resulting light travel time curtails interactive operations so that the instrument must perform most operations by programmed sequences on-board the instrument.

The SECCHI concept of operations leads to the following characteristics for image scheduling:

1) Provide for an autonomous operation for long periods of time (1 week or more)
2) Synchronize image taking between spacecraft in which every image is scheduled
3) Handle some non-image taking operations in timeline (doors and script tasks)
4) Manage timeline of image taking and events to 1 second resolution
5) Accept relative time schedules e.g Take COR1 image at 1 hour, 1 minute and 10 seconds from the current time
6) Accept absolute time schedules e.g. Take COR1 image at 12:01:10 A.M. Nov 15, 2007
7) Compact the image schedule of commands to reduce the uplink load
8) Use on-board tables to minimize the amount of information uplinked daily
9) Provide blocks of schedule commands that may be reused and called from a daily schedule
10) Provide the planned schedules as a simple text file with embedded comments to facilitate ground operations and communication via email with co-investigators.

The image scheduling software maintains a single timeline of observations for all five telescopes. The uplinked schedules are parsed and entered into the timeline either manually or automatically at midnight each day from a RAM disk file. Normally the automatic load is used. If the expected schedule is not found then a default schedule is loaded.

A normal image acquisition sequence consists of the following steps: set up the instrument mechanism configuration, clear the CCD, open the shutter for a specified time, read out the CCD and transmit the digitized signal to a buffer in the SEB, process the image for downlink. One CCD from the SCIP and one CCD from the HI can be read out at the same time. With a readout time of about 4 seconds, this is not a severe restriction. Exposures may overlap on all of the telescopes.

Schedules are designed on the ground using a software planning tool that uses the flight software tables as input. The planning tool is able to add, delete and insert images into its timeline, manage on-board resources such as RAM buffer space, downlink telemetry, computer usage, spacecraft solid state recorder

(SSR) usage, times of image exposure and image readout. The tool can merge blocks of schedule to form daily schedules. One common use is to merge a special observing program with a synoptic schedule. The planning tool also schedules door operations in anticipation of spacecraft thruster firings and script tasks used for guide telescope calibration and mechanism calibration.

10.2 Image Processing

Once an image is taken, the image is moved from the camera buffer memory to the computer for image processing. The image processing task is a background task that processes one image at a time and produces an image file ready to downlink. Since there are 27 camera buffers it is possible for image taking to take data faster than it can be processed, so the task maintains a queue of images to be processed in the order they are taken.

There are 120 image processing functions including three major types of image compression, event detection and reporting, two types of cosmic ray scrubbing, automatic exposure control, automatic compression control, occulter and region of interest masks, adding and subtracting images and the ability to send images down any of four channels (real-time, space weather, solid state recorder 1, solid state recorder 2). When the image is scheduled, image processing is selected by specifying a row from an image processing table where each row is a list of functions to be done in sequential order. There are 100 rows in the image processing table. New image processing tables can be uploaded in flight as needed.

Image compression is the most important feature of the image processing. Four types are provided including no compression. The Rice method is a lossless compression providing about a factor of 2.2 times compression. H-Compress is a lossy wavelet image compression with a variable image compression. ICER is a lossy wavelet image compression, which has the advantage of being able to specify the desired output size. ICER is predicted to produce useful images with a compression factor of up to 20. Rice and H-compress were used to compress the LASCO and EIT images and ICER was used on the Mars Exploration Rover (MER) mission.

In order to achieve the desired signal to noise ratio, the HI images require longer exposure times (about 30 minutes) than the SCIP images. To eliminate the dark current the long exposures are obtained by exposing the CCDs for short times (up to 1 minute) and then summing the desired number of images in the on-board computer. The summing involves the following steps: remove the electronic offset, scrub the images of cosmic ray impacts, perform a 2x2 pixel sum to create a 1024 x 1024 image and then add the binned image to the image sum. The cosmic ray impacts (about 45 pixels/sec) must be removed prior to summing. Two types of cosmic ray scrubbing are provided. The first does a two-image compare of each pixel of the current image to the previous image. If the current pixel is within the photon noise range of the last pixel it is accepted otherwise it is replaced with the older pixel. The second method does a three-image compare and chooses the median value. The images are then summed and added to 1024 x 1024 x 32 bit image buffers. Successive HI images, typically tens of images, are added to the image buffer until the 32 bit image buffer is sent down using Rice image compression. The cosmic ray scrubbing and image summing for HI is the single most demanding task for the on-board computer.

After image processing is done, the completed files are put on a 52 MB RAM disk for the telemetry task to send the file to the spacecraft over the MIL-STD 1553 spacecraft bus. The bus transfers roughly 1 MB per minute to the spacecraft. A full sized SECCHI uncompressed image is 8 MB in size. Using an image compression factor of 20 times means that a full sized image will downlink to the spacecraft in just 24 seconds and that the RAM buffer can hold about 120 images.

11 SECCHI Concept of Operations

11.1 Overview

The SECCHI Payload Operations Center (POC) will be located at NRL for all normal operations, except for and critical instrument debugging when it will be located at the Johns Hopkins University Applied Physics Laboratory (APL). The POC sends commands to and receives telemetry from the instrument via the Mission Operations Center (MOC), located at APL. SECCHI uses the Integrated Test and Operations System (ITOS) software hosted on Sun Blade workstations running Solaris (one for each spacecraft) for commanding and telemetry processing. Commands to be transmitted to the instrument are sent to the MOC. The MOC performs simple verification tests and then queues the commands for transmission to the spacecraft via the Deep Space Mission System (DSMS). Finally, the Command and Data Handling (C&DH) process on the spacecraft forwards the commands to SECCHI over the 1553 bus. During normal operations, commands will be sent to the MOC at least 8 hours in advance of a daily track that lasts from 3.5 to 5 hours, depending on the phase of the mission. The daily tracks are nominally centered every 24 hours for each observatory.

Most housekeeping and science data are recorded on the onboard solid-state recorder (SSR) for later transmission to the ground during the daily track. The nominal SECCHI real-time data rate is 3.6 kilobits per second (kbps), and will be used predominantly for critical housekeeping data. Real-time telemetry is forwarded immediately to the MOC, and is made available to the POC via a TCP/IP connection. All real-time and SSR playback telemetry is forwarded from the DSMS to the MOC after completion of each track. The MOC maintains an archive of all instrument telemetry for 30 days. The SECCHI POC will retrieve the telemetry daily, after the MOC has produced cleaned and merged Level-0 files. The MOC will split the daily telemetry into 6 files, each containing four hours of SECCHI telemetry. Because data for a given day may require more than one track to be completely transmitted to the ground, the Level-0 files are regenerated each day for the two preceding days. The final Level-0 files are generated by the MOC after 30 days. The SECCHI POC will download those files also. The pipeline processing will be applied daily to the quick-look Level-0 files and again after the final Level-0 files are prepared.

11.2 SECCHI Data Allocation and SSR utilization

Table 11-1 shows the peak data rate at which the C&DH collects telemetry data from SECCHI over the 1553 bus, and the SSR volume and downlink bandwidth allocated to SECCHI at various stages during the nominal two-year mission. Note that the allocations in this table are based on the average data volume guaranteed by the MOC to be downlinked during each daily track. The actual daily data volumes achieved during the mission may be higher than the nominal SSR allocations. The SECCHI SSR allocation of 6553 Mbits includes margin to account for cases where the daily tracks are separated by more than the nominal 24 hours, and is sufficient to hold up to 36 hours of data at an average SSR write rate of 50 kbps.

The SSR allocation is divided into two partitions for science data and one for space weather data. The SSR1 partition is nominally 80% of the total allocation for science data. When SSR1 partition is full, no further data may be written to it until all data on the partition has been transmitted to the ground. The SSR2 partition is nominally 20% of the total allocation for science data. The SSR2 partition functions like a circular buffer, and will overwrite the oldest data when full. The flight SW controls which packets get sent to the SSR2 and can stop writing if it detects an event trigger for example.

It is anticipated that SSR1 will be used for a synoptic program that will maintain synchronized observations on both spacecraft, and that will remain unchanged for extended periods of time throughout the mission. SSR2 will be used for special observing programs, for example those that require high-cadence observations with one or more telescopes for a short period of time. A sample synoptic program that fits within the nominal SSR1 allocation in the first 14 months on heliocentric orbit is shown in Table 11-2. These may or may not be duplicated on the other spacecraft. For example, if the trigger to stop recording is based on an on-board CME detection, there is no guarantee that both spacecraft will see the same event at the same time.

Table 11-1: SECCHI Data Rates and SSR Allocations

1553 Bus Telemetry Bandwidth Allocation		
Packets per second	70	
Peak Data Rate	152 kbps	
SSR Partitions		
SSR1	5162 Mbits	
SSR2	1291 Mbits	
Space Weather	100 Mbits	
Downlink Data Volume		
Mission Time[1]	**SSR Allocation[2]**	**Average SSR Write Rate**
Months 0-14	4742 Mbits	54 kbps
Months 14-18	4383 Mbits	50 kbps
Months 18-24	3995 Mbits	45 kbps

[1]Months after entering heliocentric orbit
[2]Includes 74 Mbits for space weather data

Table 11-2: Sample daily synoptic program for the first 14 months on heliocentric orbit

Telescope	# Images and Size (pixels)	Cadence (minutes)	Total Images/Day	Compression Factor	Total Mbits/Day
EUVI	2 1k × 1k 4 2k × 2k	4 20	576 288	10.0 10.0	845.6 1691.1
COR1	3 1k × 1k	8	540	10.0	792.7
COR2	3 1k × 1k 3 2k × 2k	15 60	216 72	10.0 10.0	317.1 422.8
HI1	1 1k × 1k	60	24	2.5	211.4
HI2	1 1k × 1k	120	12	2.5	105.7
Total			1728		4386.4

11.3 Observation Planning

The SECCHI flight software has enabled a very flexible program and supports the acquisition of over 5000 images each day for each spacecraft. The relative cadence of the various image types is the main variation that affects the planning. The basic observing philosophy for SECCHI consists of two observing programs that run simultaneously on both observatories. The first ("synoptic") program schedules every observation by time, is identical on both observatories, and occupies about 80% of the available telemetry. The second ("campaign") program is more flexible, allowing higher data rates for limited periods of time. It writes to SSR2, the overwriting telemetry buffer. Simultaneous observations from both observatories are still desirable in this mode, but are not a requirement. The lower cadence data from the synoptic program from both observatories remains undisturbed.

It is important to keep in mind that the scientific emphasis of the STEREO mission is constantly changing as the two observatories drift apart. Since observations at a specific spacecraft separation angle can't be repeated, observations must be carefully planned in advance. We will favor the EUVI observations early in the mission, when the separation angle between the observatories is small enough for stereoscopic imaging in the classical sense, and when the STEREO telemetry rate is highest due to the proximity to Earth. During that time, the EUVI will focus on CME initiation studies using high cadence imaging.

Planning for SECCHI observations will occur in multiple stages in coordination with other STEREO instruments and the MOC, with more detailed plans established at each stage. Broad science plans and priorities will be established at quarterly meetings of the STEREO Science Working Group (SWG) and at the SECCHI team meetings. The plans will be posted on the web and will be refined during monthly meetings of the Science Operations Working Group (SOWG), after which a schedule of observations will be generated. The detailed plans will be finalized at weekly teleconferences, with participation from the

spacecraft, all instrument teams and the SSC. The SECCHI observing plans for one day up to a week will be generated using the SECCHI Planning Tool. This tool is a set of Interactive Data Language (IDL) procedures that provides a graphical user interface to allow the operator to generate a file of schedule commands for both spacecraft to be sent to the MOC via the ITOS software. The planning tool performs constraint checking (for example, a warning is generated if simultaneous readouts from two CCDs controlled from the same CEB are scheduled), and monitors both internal buffer space and telemetry usage for each telescope. It is based on a similar tool that has been used in planning LASCO and EIT observations on the SOHO mission for over 10 years. The planned schedule can be displayed on the Web both in graphical format and as a text file.

11.4 Beacon Mode

SECCHI space weather data will be broadcast continuously at a rate of 504 bps over the beacon channel. These data will consist of a subset of images from each telescope. In order to fit within the low bandwidth, the images need to be highly compressed, probably binned to a low spatial resolution, as well as a subset of event messages that can be used to monitor instrument status outside of the regular track periods. The exact compression techniques will be determined after launch. The SSC is responsible for collecting these data from the various ground stations that receive them, processing the data and serving them on the Web.

11.5 SECCHI Campaigns

For two or more periods totaling four weeks during the mission, there will be an additional track lasting 1.75 hours each day, beginning12 hours after the start of the normal daily track. These 'SECCHI Campaigns' will be used to downlink additional SECCHI data, and will enable high-cadence observations targeted to specific science objectives. The other instruments will continue to receive their normal daily data volumes during these times.

11.6 Routine Processing and Data Products

Routine processing of SECCHI data will take place at the POC (for real-time and socket playback data) and at the SECCHI Data Processing Facility (DPF, for Level-0 packet files) at NRL. Science data will be processed into FITS files, consisting of a binary data array preceded by a header, with one file per image. No calibrations will be applied to the data during routine processing, and the resulting FITS file will be referred to as Level-0.5. FITS files generated from real-time data are referred to as 'quick-look'. FITS files generated from socket playback or Level-0 files will be referred to as 'preliminary'. When the final Level-0 files are available from the MOC after 30 days, the resulting FITS files will be referred to as 'final'. All final Level-0.5 FITS files will be archived at NRL, and will also be delivered electronically to the SSC and to Co-Investigator institutions. Processing of data to Level-1 and higher levels will be done by individual users, using IDL routines and auxiliary data that will be freely distributed as part of the SolarSoft software library and database. Some higher level data products, such as polarized brightness images from COR1 and COR2, and Carrington maps, will be generated routinely by the DPF. Additional data products, including browse images, movies, lists of events such as CMEs and comets, housekeeping tables and long-term trending plots of key instrument performance parameters will also be generated routinely and made available electronically.

11.7 SECCHI Data Policy

The SECCHI data policy is to have completely open access to all data, including the calibration data and procedures necessary to calibrate and process the data to higher levels. SECCHI images will be available as soon as the routine processing steps have been completed. This is estimated to be within 30 minutes of receipt of all data necessary to form an image. The image data will be accessible via the Web using a searchable database. It will be possible to generate queries to select and download data of interest using FITS header keywords as parameters. Temperatures, voltages, and other housekeeping parameters will also be accessible through database queries.

ACKNOWLEDGEMENTS

We gratefully acknowledge the hard work and dedication of the literally hundreds of people who contributed to the SECCHI program. The SECCHI instrument was constructed by a consortium of institutions: the Naval Research Laboratory (NRL, Washington, D.C., USA), the Lockheed Solar and Astrophysical Laboratory (LMSAL, Palo Alto, CA, USA), the NASA Goddard Space Flight Center (GSFC, Greenbelt, MD, USA), the Max Planck Institüt für Sonnensystemforschung (MPS, Lindau, Germany), the Centre Spatial de Liege (CSL, Angleur, Belgium), the University of Birmingham (UB, Birmingham, UK), the Rutherford Appleton Laboratory (RAL, Didcot, UK), the Institut d'Optique (IOTA, Orsay, France), the Institute d'Astrophysique Spatiale (IAS, Orsay, France).

NRL is the lead institution in the consortium and was responsible for the supplying the COR2 coronagraph, the experiment electronics, the CCDs and focal plane assemblies, the flight and ground software, the integration and testing of the instrument and the overall program management. LMSAL was responsible for providing the EUVI telescope, the GT, the mechanism electronics box and mechanisms for the COR1, COR2 and EUVI shutters and wheels. The GSFC was responsible for providing the COR1 telescope.

The USA effort was supported by the NASA Solar Terrestrial Physics STEREO Program under DPR S-13631-Y. The program managers at GSFC were Abby Harper, Haydee Moldanado and for the last 3 years of the program, Nicholas Chrissotimos. The program manager for instruments was Michael Delmont and the SECCHI instrument manager was Bernie Klein. We are indebted to their efforts and to those of the other members of the STEREO project. The NRL effort was also supported by the USAF Space Test Program and the Office of Naval Research.

Add statements regarding European support.

REFERENCES

Akin, D., R. Horber, C.J. Wolfson, Three High Duty Cycle, Space-Qualified Mechanisms, NASA Conf. Pub. 3205, 1993.

Allen, C.W., Astrophysical Quantities, Springer-Verlag, New York, ISBN 0387987460, 2000.

Billings, D. E. (1966). A Guide to the Solar Corona. New York: Academic Press.

Buffington, A. Jackson, B.V., Korendyke, C.M., Applied Optics, Vol 35, pp.6669-6673, 1996.

Defise, J., Halain, J., Mazy, E., Rochus, P. P., Howard, R. A., Moses, J. D., Socker, D. G., Harrison, R. A. & Simnett, G. M., Design and tests for the heliospheric imager of the STEREO mission, in 'Innovative Telescopes and Instrumentation for Solar Astrophysics', Eds S.L. Keil, S.V. Avakyan . Proc SPIE 4853, 12-22, 2003.

Delaboudinière, J. P. et al., EIT: Extreme-Ultraviolet Imaging Telescope for the SOHO Mission. Solar Phys. Vol. 162, pp 291-312, 1995.

Eyles, C.J., Simnett, G.M., Cooke, M.P., Jackson, B.V., Buffington, A., Hick, P.P., Waltham, N.R., King, J.M., Anderson, P.A., Holladay, P.E., *Solar Phys.*, 217, 319-347, 2003.

Gibson, E. G. (1973). The Quiet Sun. SP-303. National Aeronautics and Space Administration.

Handy, B. N. et al., The Transition Region and Coronal Explorer, Solar Phys. Vol 187, pp. 229-260, 1999.

Harrison, R.A., Davis, C.J., Eyles, C.J., The STEREO Heliospheric Imager: How to detect CMEs in the heliosphere, Adv. Space Res. 36, 1512-1523, 2005.

Howard, R.A., Moses, J.D., Socker, D.G., and the SECCHI consortium, Sun Earth Connection Coronal and Heliospheric Investigation (SECCHI), in 'Instrumentation for UV/EUV Astronomy and Solar Missions', (eds) S. Fineschi, C.M. Korendyke, O.H. Siegmund, B.E. Woodgate, SPIE (Washington) 4139, 259-283, 2000.

Koutchmy, S. and Lamy, P.L., The F-corona and the circum-solar dust evidences and properties, in 'Properties and Interactions of the Interplanetary Dust' (eds) R.H. Giese and P. Lamy, IAU Colloq. 85, 63, D. Reidel, Dordrecht, ISBN 90-277-2115-7, 1985.

Lyot, B. (1939). The study of the solar corona and prominences without eclipses (George Darwin Lecture, 1939). Mon. Not. Royal Astron. Soc., 99, 580–594.

Morrill, J.S. et al, Calibration of the SOHO/LASCO C3 White Light Coronagraph, Sol. Phys. Vol. 233, 331-372, 2006.

Norton's Star Atlas, (ed) I. Ridpath, Longman, London, ISBN 0582312833, 1998.

Pike, C.D. and Harrison, R.A., Long-duration cosmic ray modulation from a Sun-Earth L1 orbit, *Astron. Astrophys.*362, L21-L24, 2000.

Ravet, M. F., F. Bridou, X. Zhang-Song, A. Jerome, F. Delmotte, M. Bougnet, JP. Delaboudinière, Ion beam deposited Mo/Si multilayers for EUV imaging applications in astrophysics, Proc. SPIE Vol. 5250, 2003.

Socker, D.G., Howard, R.A., Korendyke, C.M., Simnett, G.M., Webb, D.F., The NASA Solar Terrestrial Relations Observatory (STEREO) mission Heliospheric Imager, in 'Instrumentation for UV/EUV Astronomy and Solar Missions', (eds) S. Fineschi, C.M. Korendyke, O.H. Siegmund, B.E. Woodgate, SPIE (Washington) 4139, 284-293, 2000.

Stern, R. A., L. Shing, M.M. Blouke, Quantum efficiency measurements and modeling of ion-implanted, laser-annealed charge coupled devices: x-ray, extreme-ultraviolet, ultraviolet, and optical data. Appl. Opt. Vol. 33, pp. 2521-2533, 1994.

Stern, R. A. and the SXI Team, Solar X-ray imager for GOES, Proc. SPIE Vol. 5171, 2003

Strong, K., Bruner, M, Tarbell, T., Title, A., Wolfson, C., TRACE-The transition region and coronal explorer, Sp. Sci. Rev., Vol. 70, 119 (1994).

Thompson, W. T., Davila, J. M., Fisher, R. R., Orwig, L. E., Mentzell, J. E., Hetherington, S. E., Derro, R. J., Federline, R. E., Clark, D. C., Chen, P. T. C., Tveekrem, J. L., Martino, A. J., Novello, J., Wesenberg, R. P., StCyr, O. C., Reginald, N. L., Howard, R. A., Mehalick, K. I., Hersh, M. J., Newman, M. D., Thomas, D. L., Card, G. L., and Elmore, D. F. (2003). COR1 inner coronagraph for STEREO-SECCHI. In Keil, S. L. and Avakyan, S. V., editors, Innovative Telescopes and Instrumentation for Solar Astrophysics, volume 4853 of Proc. SPIE, pages 1–11.

Windt, D. L. and R.C. Catura, Multilayer Characterization at LPARL, Proc. SPIE Vol. 984, pp. 132-139, 1988.

Wülser, J-P. et al., EUVI: the STEREO-SECCHI Extreme Ultraviolet Imager, Proc. SPIE Vol. 5171, 2003.

Young, P. R., G. Del Zanna, E. Landi, K.P.Dere, H.E. Mason, M. Landini, CHIANTI – An Atomic Database for Emission Lines. The Astrophys. Journal Suppl. Series Vol. 144, pp. 135-152, 2003.